On the quality of RS41 radiosonde descent data

Bruce Ingleby[1], Martin Motl[2], Graeme Marlton[3], David Edwards[3], Michael Sommer[4], Christoph von Rohden[4], Holger Vömel[5], Hannu Jauhiainen[6]

[1]European Centre for Medium-Range Weather Forecasts, Reading, RG2 9AX, UK
[2]Czech Hydrometeorological Institute, Prague, 14306, Czechia
[3]Met Office, Exeter EX1 3PB, UK
[4]Deutscher Wetterdienst (DWD)/GCOS Reference Upper Air Network (GRUAN) Lead Center, Lindenberg, Germany
[5]National Center for Atmospheric Research, Boulder CO, 80301, USA
[6] Vaisala Oyj, 01670 Vantaa, Finland

Correspondence to: Bruce Ingleby (bruce.ingleby@ecmwf.int)

Abstract. Radiosonde descent profiles have been available from tens of stations for several years now - mainly from Vaisala RS41 radiosondes. They have been compared with the ascent profiles, with ECMWF short-range forecasts and with co-located radio-occultation retrievals. Over this time our understanding of the data has grown, and the comparison also shed some light on radiosonde ascent data. The fall rate is very variable and is an important factor, with high fall rates being associated with temperature biases, especially at higher altitudes. Ascent winds are affected by pendulum motion, on average descent winds are less affected by pendulum motion and are smoother. It is plausible that the true wind variability in the vertical lies between that shown by ascent and descent profiles. The discrepancy indicates the need for reference wind measurements. With current processing the best results are for radiosondes with parachutes and pressure sensors. Some of the wind, temperature and humidity data are now assimilated in the ECMWF forecast system.

1 Introduction

Radiosondes were first developed in the 1930s and have been used to measure profiles of temperature, humidity and wind since then. There are approximately 800 operational radiosonde stations worldwide, mostly providing ascents once or twice per day. These are used for Numerical Weather Prediction (NWP), climate studies and other applications. The Global Climate Observing System (GCOS) set up the GCOS Reference Upper-Air Network (GRUAN) to produce reference quality data, with uncertainty estimates, from a subset of stations (Bodeker et al, 2016). Climate users, like GRUAN, tend to focus on temperature and humidity. For NWP the winds are arguably more important (shown for aircraft data by Ingleby et al, 2021) - partly because satellites provide more temperature and humidity information than wind information. One attraction of radiosonde descent data is that there is very little additional cost involved and potentially an extra vertical profile, assuming that the quality is acceptable. Whilst performing this study, it has become apparent that descent data prompts a re-examination of ascent data and this can either support or challenge our views of the ascent data.

We have found two previous published studies of radiosonde descent data – with different types of radiosonde. Tiefenau and Gebbeken (1989) compared ascent and descent temperatures and found the descent values to be higher at upper levels. They took the descent temperatures as accurate and suggested that the ascent temperatures were too low due to sampling the balloon wake and adiabatic cooling of the gas within the balloon. Whilst wake effects cannot be completely discounted, our results suggest that the descent temperatures are too high. Using Meisei radiosondes at a station in southern India Venkat Ratnam et al. (2014) found similar ascent/descent temperature differences and advised some caution while using the descent data; in particular "Note that descent rate is quite high (50–60 m s^{-1}) immediately after balloon burst, and it takes some time to stabilize. Thus, the data within a few kilometers from the balloon burst may be biased because of improper sampling." Venkat Ratnam et al. (2014) used the radiosonde dimensions to estimate drag and hence the descent rate but there are unknowns (orientation and the mass of the balloon still attached) and the actual descent rates were lower (their figure 6).

As radiosondes are designed to measure during the ascent, it is useful to consider how they differ from dropsondes which always measure on descent. Dropsondes are launched from aircraft and are mainly used for sampling around tropical cyclones and for field experiments. Radiosondes typically have the temperature and humidity sensors mounted diagonally above the radiosonde body whereas dropsondes (e.g. Hock and Franklin, 1999) have the sensors underneath - in each case to sample air undisturbed by the radiosonde body. The AVAPS (Advanced Vertical Atmospheric Profiling System) processing system used by many dropsondes includes an 'inertial' correction for the delayed response to horizontal wind shear (Appendix of Hock and Franklin, 1999). Modern radiosondes are usually on a line 30-55 m below the balloon whereas dropsondes are only 1 m or less below a parachute. As noted by Wang et al (2008) 'The dropsonde fall rate is much smoother than the radiosonde ascent rate because of the radiosonde's pendulum effect and self-induced balloon motion'. Typically dropsondes fall at about 10 m s^{-1}, just after launch it can be about 20 m s^{-1} before the parachute opens fully. As discussed below, radiosonde descent can be much faster (to 100 m s^{-1} or more if no parachute is used) shortly after balloon burst. There has been some use of controlled descent, by partial deflation of the balloon, for measurement of stratospheric humidity (Hurst et al, 2011). Zhang et al (2019) tested the use of a low density 'hard ball' to give more consistent drag than a parachute when deriving the vertical velocity of the air using a radiosonde descending from a height of about 10 km.

Figure 1 shows BUFR (Binary Universal Form for Representation of meteorological data) descent reports over Europe for September-November 2019 (descent data were also available from New Zealand, not shown). BUFR allows the reporting of high vertical resolution radiosonde data (Ingleby et al., 2016). Geller at al., (2021) found that in mid-2020 44% of operational radiosonde stations were providing high vertical resolution ascent data. Since 2019 descent data has become available from more European stations and a few in the Americas. After launch the balloon is advected horizontally by the wind, especially at upper levels, and typically travels 50 to 300 km before burst with the larger distances being more common in winter (Seidel et al., 2011).

Sep-Nov 2019: Descent data BUFR availability/type
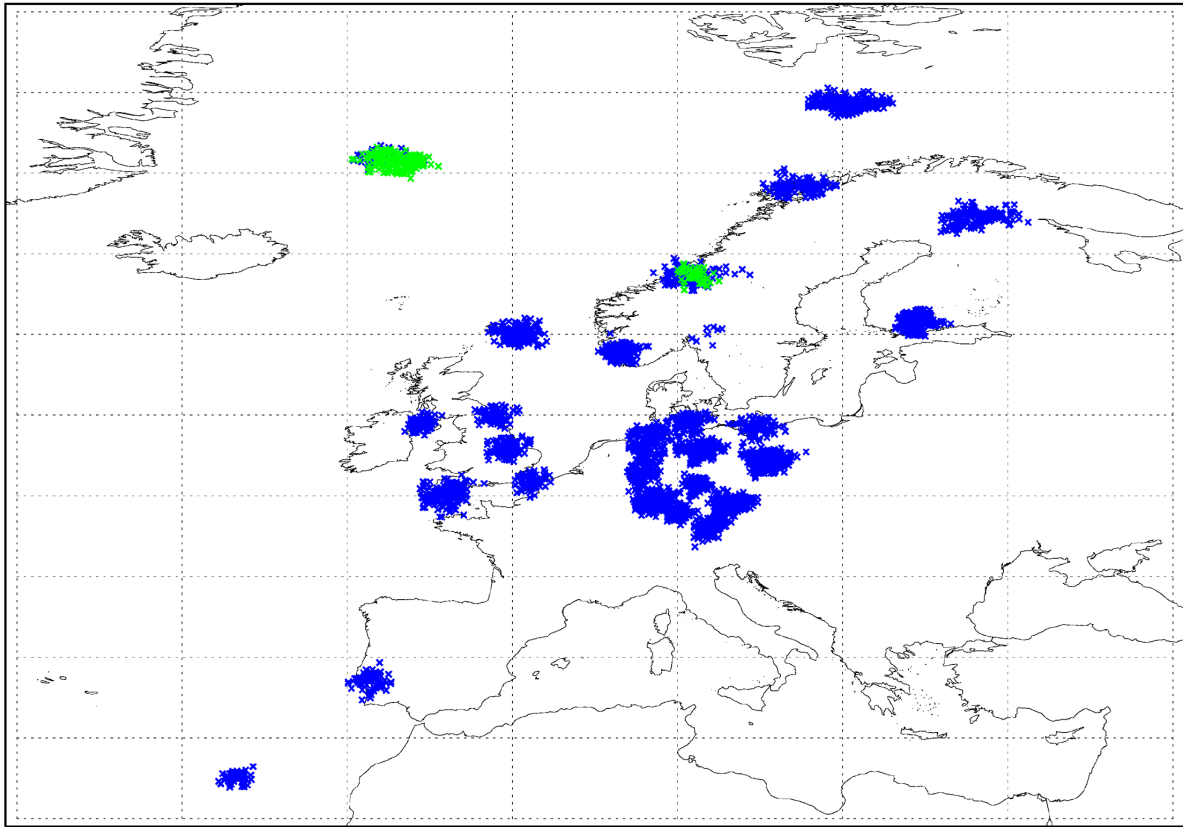
Figure 1: Descent reports (burst positions) over Europe for September-November 2019, blue - Vaisala RS41, green - Modem M10. There were 14 stations from Germany, 6 each from UK and Norway and 2 each from Finland and Portugal.

Figure 2 gives an indication of the number and vertical extent of descent profiles. Larger balloon size and fill volume is used to achieve higher altitudes. On average, radiosondes that achieve higher altitudes drift further horizontally, resulting in the radio signal to the launch station being lost at higher altitudes on descent due to obstruction by terrain or signal attenuation. This can be seen clearly in the UK results which have been split into automatic and manual launches: the manual launches use larger balloons and the number of descent reports starts to decline earlier, below 9 km. Automatic launchers are documented by Madonna et al. (2020). Some of the other countries use a mixture of manual and automatic launchers, but with little or no difference in balloon size. Some ascents, usually less than 5%, do not have a corresponding descent report, often due to a fault developing with the radiosonde before or upon burst, leading to an automatic termination.

.

Country	Parachute	Pressure sensor	Balloon weight (g)
Norway	No	Yes	350 (01004*: 1500)
Finland	No	No	350
UK	Yes	No	350 (03005, 03808: 800+)

Germany	Yes	Yes	600 (also 300, 800) (10962: 1200+)
Portugal	Yes (2 stations)	Yes	600
New Zealand	No	No	350
Czechia	No	No	800

Table 1. Summary of metadata for countries providing descent data in 2019. For balloon weight the most common value is given followed by others used in brackets, usually with an indication of the stations involved. (* station 01004 did not provide descent reports in 2019. The names/locations of the stations can be found in https://oscar.wmo.int/oscar/vola/vola_legacy_report.txt.) The Czech data were not provided to ECMWF in real time but they are analysed in Section 4.
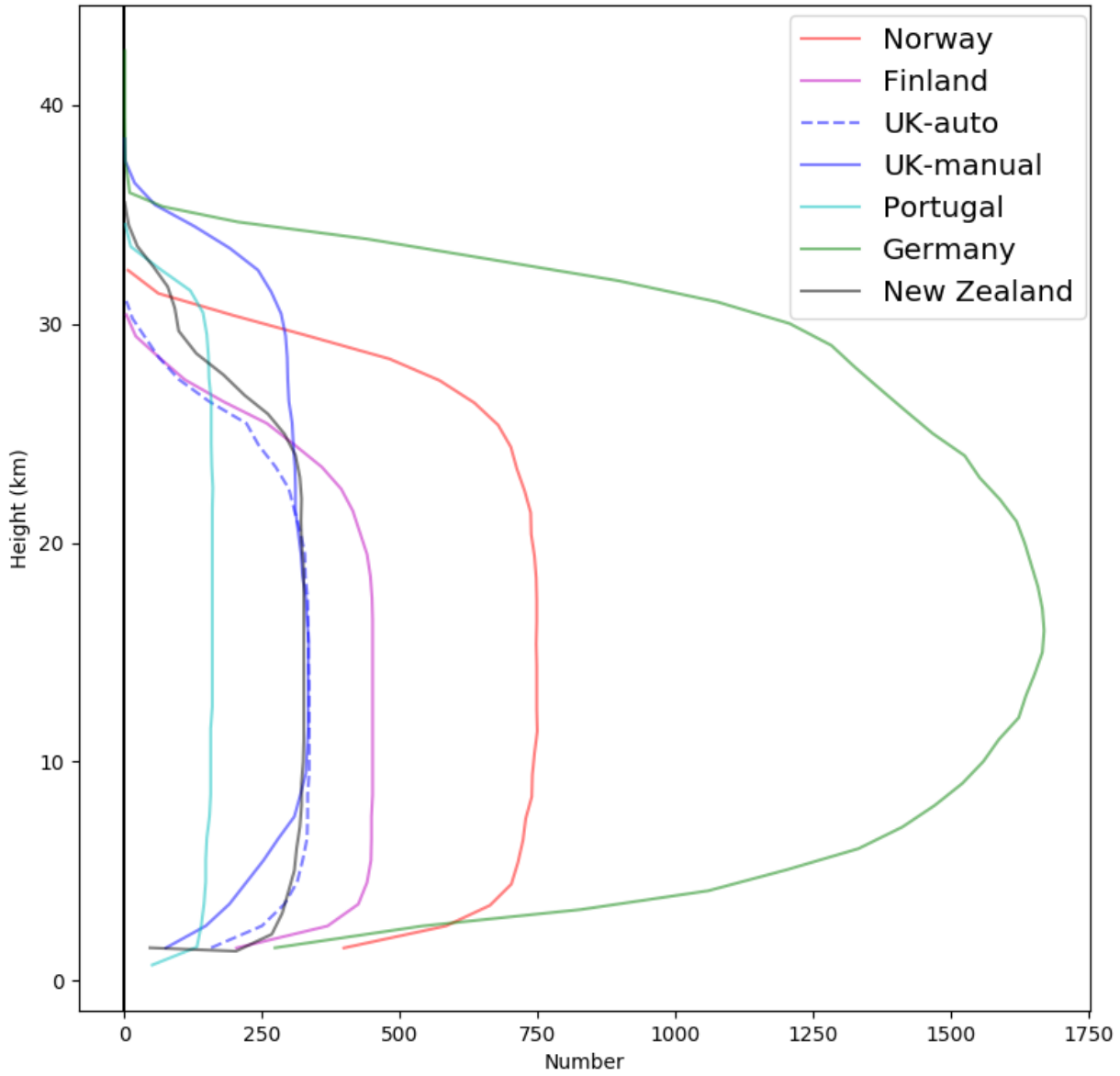
Figure 2: Numbers of RS41 descent reports by height and country, September-November 2019.

2 Radiosonde ascent and descent

2.1 What goes up must come down

A balloon is filled with hydrogen or helium and ascends, attached by a string to the radiosonde (instrument package). Balloon techniques are documented by WMO (2018b). The Vaisala RS41-SG radiosondes have a small sensor boom with temperature and humidity sensors near the end, and wind and position are measured using a GPS receiver. Some models have a pressure sensor, identified as the RS41-SGP (pressure is discussed in section 4.2). The measurements are transmitted back to the ground station and processed there. Dirksen et al (2014) describe the GRUAN processing of the Vaisala RS92 and the instrument accuracy; the operational BUFR reports come from the Vaisala processing. The Vaisala RS41 is the successor to the RS92 and is similar in many respects, but with improved humidity and temperature measurements (Edwards et al, 2014; Jensen et al, 2016). As the balloon ascends it expands in diameter and eventually bursts causing the radiosonde to descend - transmission of the measurements continues but traditionally processing stops at this point. When the radiosonde falls below the horizon as seen from the ground station then it is no longer possible to receive the transmissions. Typically, the ascent takes 90-120 minutes (reaching altitudes of 30 or 35 km) and the descent takes 30 minutes or less. The upper part of the descent is close to the upper part of the ascent in both time and space, usually with increasing separation as the radiosonde descends.

Some operators include a parachute, either inside or just below the balloon. The parachute slows the descent and is intended to reduce the risk of damage to life and property when the radiosonde reaches the surface. In sparsely populated or island countries a parachute may not be used.

From rare images of the balloon burst and recovered radiosondes (Figure 3 and supplement), and also from the motion on descent it is clear that a) sometimes the balloon bursts completely or tears off at the nozzle and the parachute opens fully, b) sometimes the balloon tears open leaving strips attached, these may get tangled with the parachute - which may partially 'free itself' later, c) sometimes the parachute ruptures and so is ineffective. Where there is no parachute we speculate that sometimes the remains of the balloon act to slow the descent. Note also that when complete, the mass of the balloon is typically several times that of the radiosonde (larger balloons are used to reach higher altitudes, they are also sometimes used at night; the same balloon/amount of gas will reach higher in the daytime on average). Some stations add extra instruments periodically, for example once a week Lerwick (03005) measures ozone as well and a larger balloon and parachute are used.
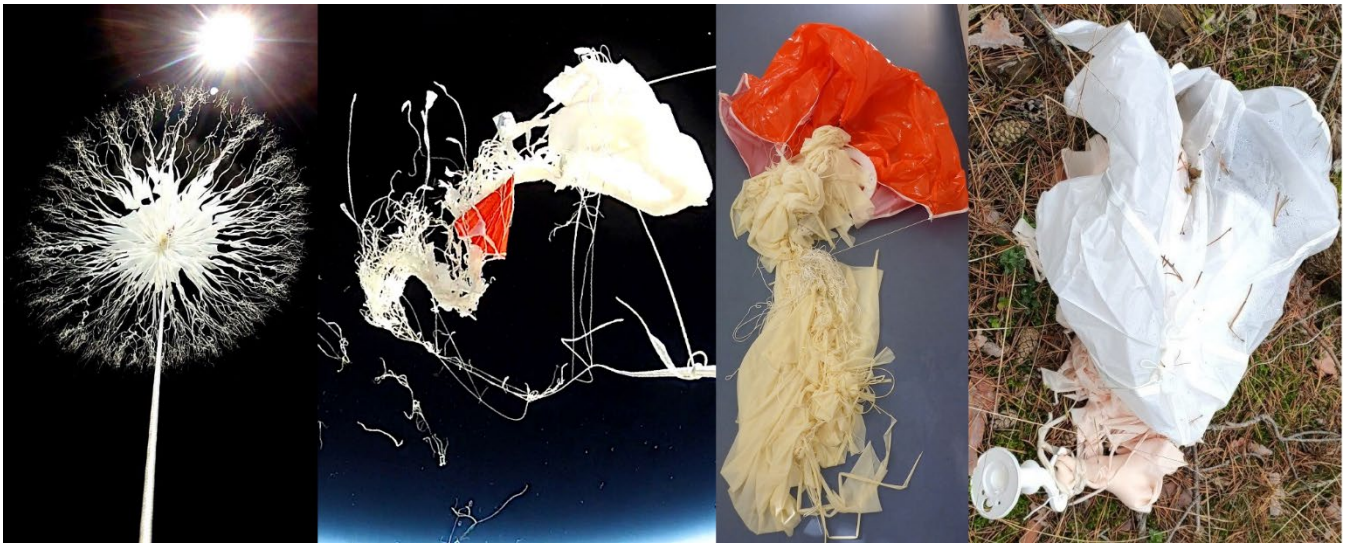
Figure 3. Left: photographs of a bursting balloon and parachute (orange) entangled in balloon remains. Right: two images of balloon remains and parachutes (orange/white) after the descents. These images are for frostpoint hygrometer launches from Lindenberg and so use larger balloons than a regular radiosonde launch.

On ascent the sensor boom projects above the radiosonde, so that it samples air that has not flowed over the body of the radiosonde. On descent, with a working parachute, it should be in a similar position - so it may sample air that has flowed over the radiosonde body, which has the potential to introduce biases or contamination. It is not known how a radiosonde descending without a parachute is orientated, or if it may be tumbling.

2.2 Types of parachute and string length

For some manual launches a parachute (if used) is attached to the line not far below the balloon. Sometimes the two can become entangled after balloon burst. For automated launches a parachute (if used) is stored within the balloon and this seems to cause fewer entanglement problems. This can be used for manual launches too, and has been used at Lindenberg for some years, but there is a small additional expense. In general, most of the parachutes are quite basic and do not include a hole. Air can build up inside the parachute and suddenly spill out. It is clear from some of our results that parachutes do not always open as intended.

In earlier decades the string connecting the balloon and the radiosonde may have been 10 m or less, but in the stratosphere the balloon gets larger and there can be intermittent influences of the balloon wake upon the instruments (WMO, 1994; Luers and Eskridge 1998; Söder et al 2019). For this reason longer suspensions are used now, WMO (2018a) suggests 40 m for radiosondes ascending to 30 km or higher. In practice an 'unwinder' is used to increase the line length shortly after the radiosonde launch (WMO, 2018b). The Vaisala unwinder for the RS41 gives 55 m when extended (Vaisala, 2017). We note

7

133 that while longer lines benefit stratospheric temperature measurements they cause larger amplitude pendulum motion in the
134 winds.

2.3 Preparation of profile reports

136 Data values are transmitted to the ground receiver every second and are processed by Vaisala MW41 software. Raw data
137 values, both ascent and descent, indexed by time are stored locally (the GRUAN archive makes the one second data available
138 for GRUAN sites). The MW41 software looks for a sustained decrease in altitude to determine the time of burst. In the past,
139 all later data would usually have been discarded but there is now an option to continue processing and to produce a separate
140 BUFR descent message using sequence 3 09 056 (WMO, 2019) designed for descent data. In 2019, as an interim measure, the
141 dropsonde sequence 3 09 053 was being used. As the timeliness of ascent data is critical for data users, it is preferable to
142 transmit the ascent profile as soon as possible after burst, followed by the descent data sent once the profile is completed.
143 BUFR from the European stations involved in this study is generally provided every two seconds (about 10 m separation in
144 the vertical during ascent).
145 The MW41 horizontal winds are derived primarily from Doppler processing of the Global Positioning System (GPS) signals
146 but the GPS locations are also used (GRUAN processing only uses the GPS positions). There is very good vertical resolution
147 but it also means that the winds sample the pendulum motion of the radiosonde - this is probably a mixture of planar and
148 conical pendulum motion. The period of the pendulum motion is a function of the length of line between the balloon or
149 parachute and the radiosonde. The processing attempts to filter out the pendulum motion (discussed briefly in Dirksen et al
150 2014), but the filtering is imperfect as discussed below.

2.4 Descent fall rates

152 The balloon and gas are chosen so that the ascent rate is about 5 m/s on average - however there is usually notable high
153 frequency variability probably due to pendulum motion. Especially in the stratosphere, there can be lower frequency signals
154 due to gravity waves and both of these features can be seen in Figure 4 (grey line, ascent). After the balloon bursts the
155 radiosonde falls very fast (over 70 m s^{-1} in this case) and then slows abruptly - presumably when the parachute opens fully.
156 After this there is a little high frequency variability (but much less than on the ascent) and a gradual decrease in descent rate
157 as the air density increases. Looking at a sample of Lindenberg descents over several weeks (see supplement), some exhibit
158 an abrupt deceleration and others do not. Figure 5 shows descent rates from the station at Sola in Norway, without parachutes.
159 These do not show the abrupt deceleration, but do show a large range of descent rates. The slower descents tend to have larger
160 high frequency variability. We tentatively suggest that in these cases, the remains of the balloon are acting to slow the descent
161 and there is some pendulum motion. Venkat Ratnam et al. (2014) suggested that the balloon remains sometimes act as a
162 parachute. The variability in the descent rate may be due to variability in the mass and shape of balloon remnants.
163 Mean descent rates by country are shown in Figure 6 (an indication of the variability is shown for Germany). For any particular
164 altitude those from Germany and the UK are slowest, reflecting their use of parachutes. Amongst the others there is a large

range. The Norwegian radiosondes fall faster than those from the other countries studied - it is unclear why they fall faster than the Finnish radiosondes. In section 3 we focus on the four northern European countries (Norway, Finland, UK and Germany) because they have similar upper air climatologies but different instrument characteristics. For Germany and Finland the descent data received at ECMWF stopped on about 20 November 2019 linked to the move to the new BUFR template. During 2020 the volume of descent profiles increased overall (e.g. France and Spain started sending them), although there was also some disruption from the Covid pandemic.
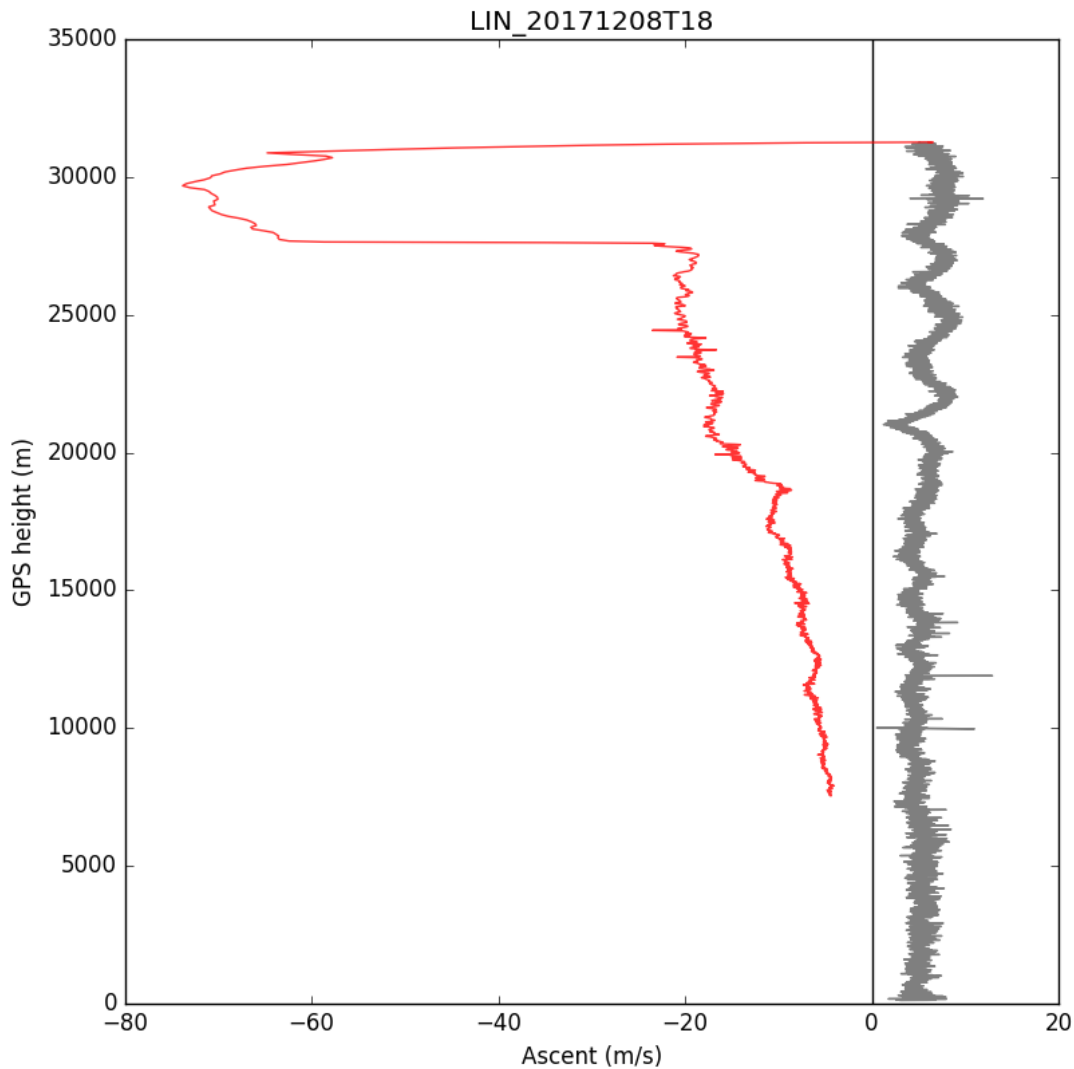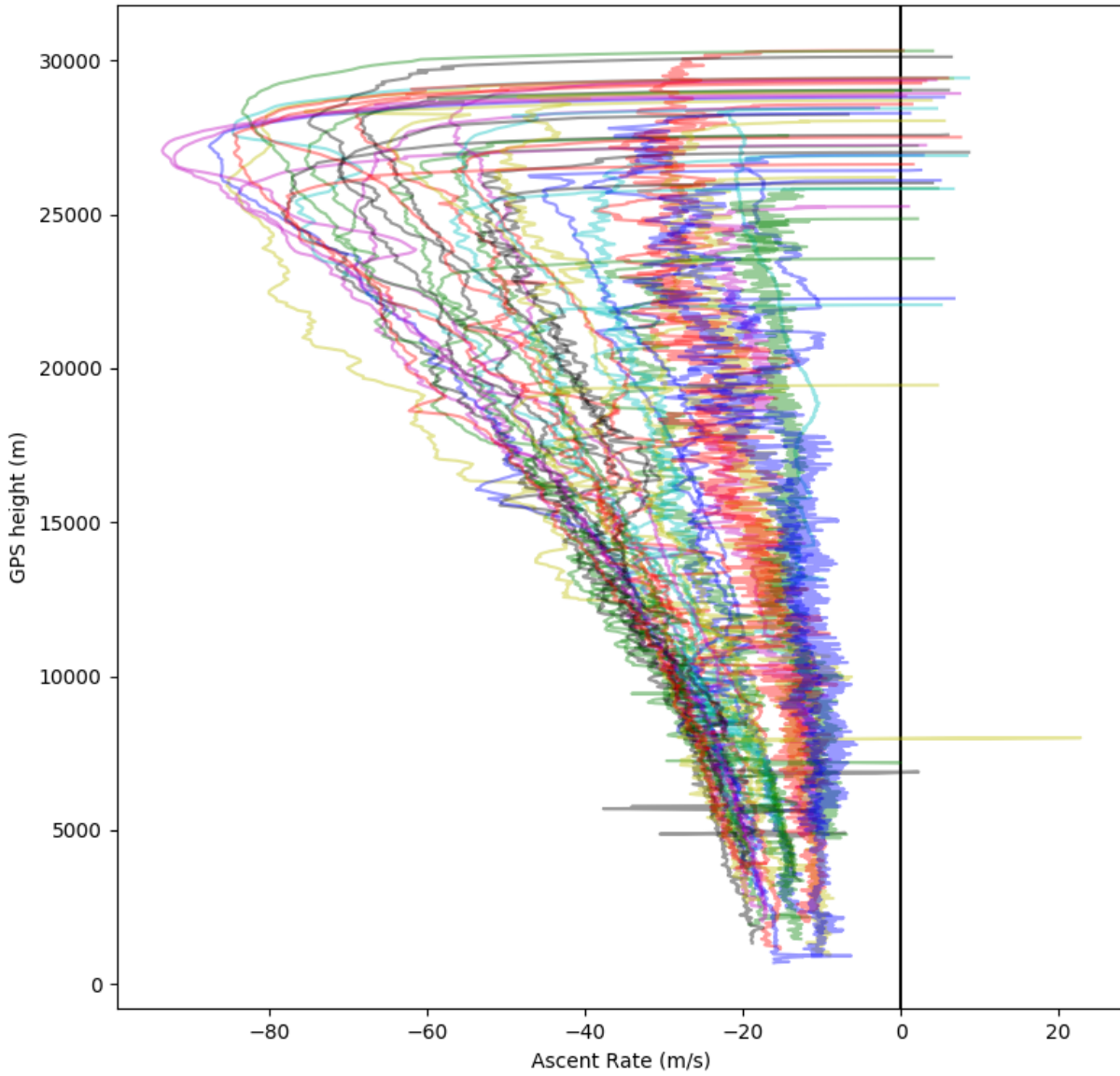

Figure 4: Ascent (grey) and descent (red) rate - an example from Lindenberg (1 s data).

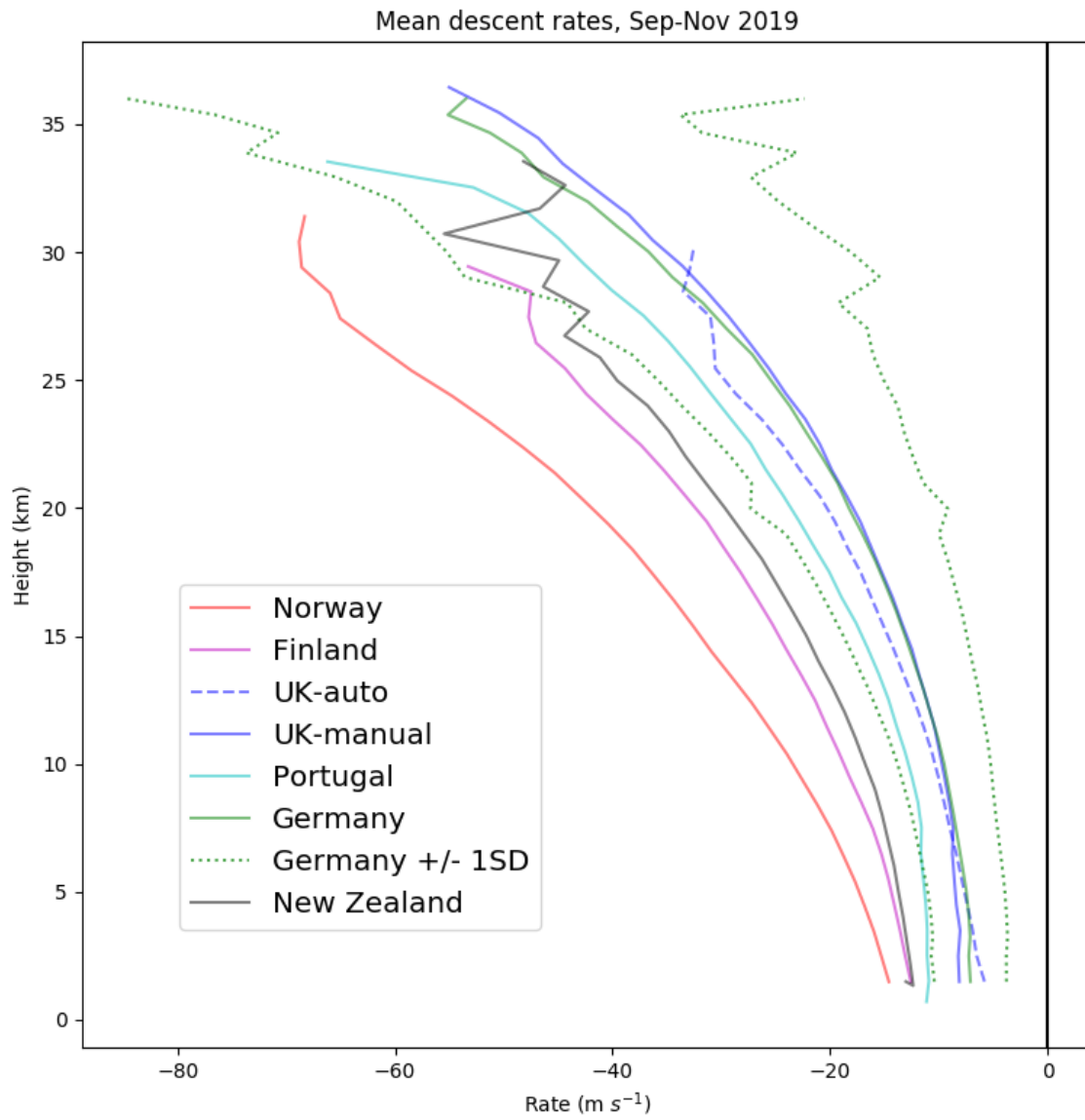**Figure 5: Descent profiles from Sola (Norway, data courtesy of Terje Borge): 14 December 2019 - 5 January 2020.**

176

177

10

Figure 6: Mean descent rates for September-November 2019, same categories as Figure 2. For German profiles an indication of the standard deviation (SD) has been provided.

2.5 Motion of radiosonde during descent

A radiosonde as it ascends through the atmosphere can be thought of as a pendulum with a moving pivot (Marlton et al, 2015). As the radiosonde encounters small scale turbulence which is ubiquitous in our atmosphere it causes the radiosonde beneath to swing. The periodicity τ is a function of string length l given by

$$\tau = 2\pi \sqrt{\frac{l}{g}}, \quad (1)$$

where g is the acceleration due to gravity. Different radiosonde manufacturers supply different string lengths for their radiosondes, with the aim of removing the radiosondes sensors from the wake effects (Luers & Eskridge 1998). The standard string length on the Vaisala RS41 is 55 m (Vaisala 2017) which gives an approximate period of oscillation 14.9 seconds and an oscillating frequency of approximately 0.07 Hz. Differing balloon sizes and the inclusion of a parachute may alter l and therefore τ slightly, a +/- 5m variation of l affects τ by +/- 0.7 s. Given the non-linear relationship in eq 1 a similar length addition for a radiosonde with a shorter tether for example will have a larger change on the period of oscillation. Depending on the operating practices the radiosonde may be launched in three broad configurations: i) No parachute; the radiosonde freefalls with some drag from the balloon remnants, ii) Balloon bursts above the parachute and radiosonde descends on the parachute and iii) The balloon contains a parachute which then deploys above the neck of the balloon and similarly descends. In addition to this, the deployment of the parachute is not consistent, see Figure 4 and Figures S4 and S5 in the supplemental material.

Marlton (2016) performed a spectral analysis of raw GPS wind measurements from Vaisala RS92 radiosonde ascents equipped with motion sensors described in Harrison and Hogan (2005) and Marlton et al (2015) and found oscillatory modes detected by the motion sensors were present in the raw GPS data. In this section raw GPS ascent and descent data from UK Met Office Autosonde sites and manned stations are used to generate Lomb Periodograms of the raw horizontal wind components.

Due to radiosondes often travelling 4-5 times their vertical ascent height in the horizontal there are on occasion small data gaps due to transmission drop out. The issue becomes more noticeable in descent data as the radiosonde is now even further from its ground station. This means a traditional Fourier transform method is not appropriate. Thus, a Lomb periodogram is chosen (Lomb 1979), which can generate periodograms which have irregularly sampled data. To ensure that we focus on the motion of the radiosonde we use the processed horizontal wind components to remove the wind field from our raw GPS readings leaving the motion of the radiosonde beneath that balloon.
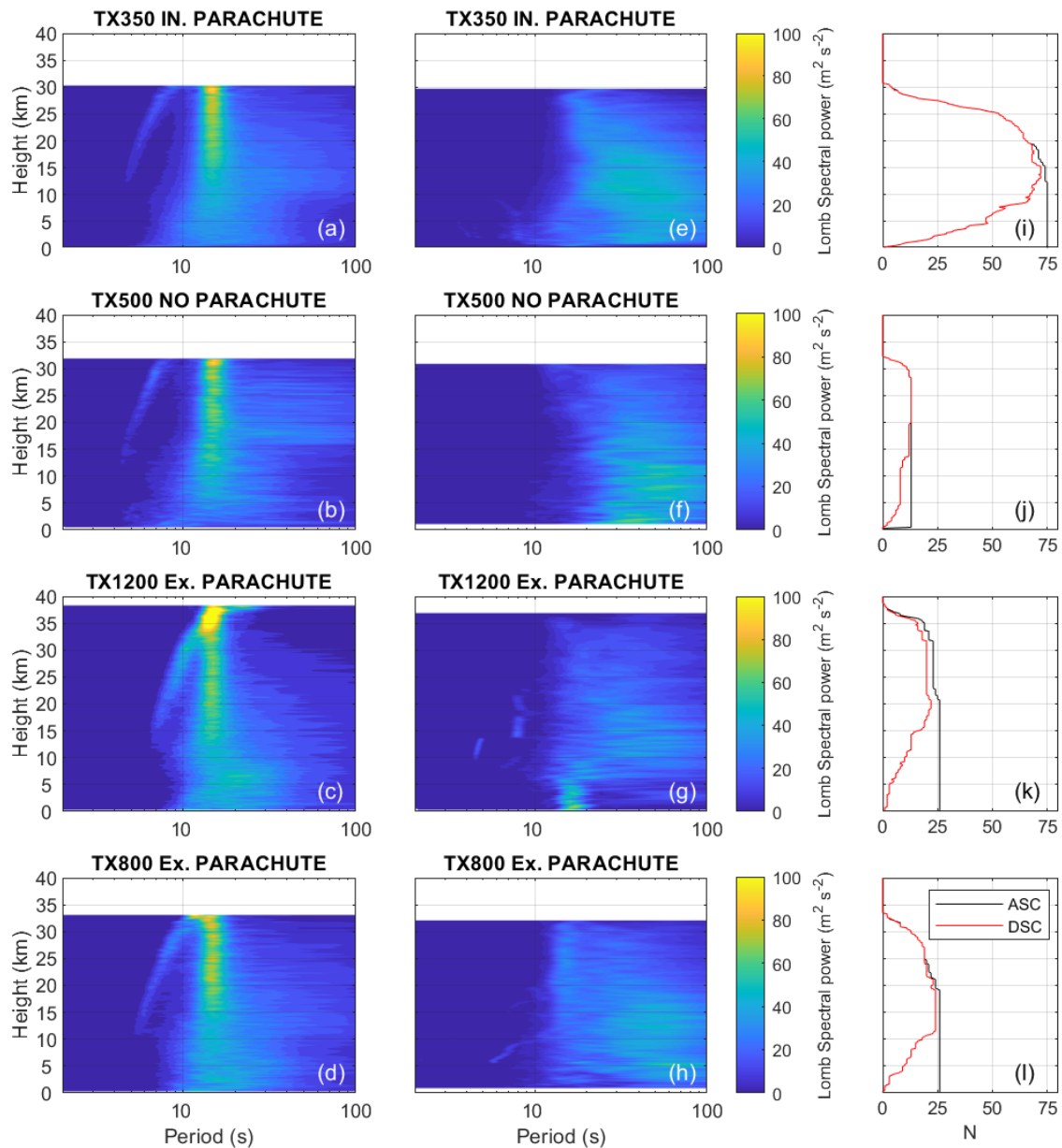
212

213   Figure 7. Composite Lomb Periodograms of detrended horizontal GPS data as a function of height for ascent data from RS41's

214   with the following launch configurations a) TX350 balloon with internal parachute, b) TX500 with no parachute, c) TX1200

215   with external parachute (day time only) and d) TX800 with external parachute. Panels e-h show composite Lomb periodograms

216   of descent data from the balloon configurations a-d respectively. Profile contributions for balloon configurations a-d during

217   ascent (descent) are shown in black (red) in panels i-l respectively.

218

219 Figure 7 a-d shows Lomb periodograms of the detrended horizontal GPS during an ascent for four different RS41 launch
220 configurations, in each case there is a dominant oscillatory period of 15 s (0.06 Hz) which strongly dominates above 15 km.
221 Examining the results from Eq (1) given the RS41's string length shows that on ascent the radiosonde and balloon are behaving
222 as a pendulum with a moving pivot.

224 During descent the oscillatory motion is very different, there is no longer a dominant oscillatory period and the amplitudes of
225 these oscillations are smaller. A general trend is that in the early stages of the descent the radiosonde is still oscillating with a
226 period of 15 s (0.06 Hz). As it falls the peak period of oscillation increases to 25-30 s, until the height of 15-20 km. At this
227 approximate height the RS41s without parachutes (panel (e)) exhibit a narrow spectral width with the smallest descent to
228 descent variability. An oscillation is still present indicating that some of the balloon remnants are acting as a parachute. For
229 the parachuted RS41s the spectral width in oscillation widens significantly indicating that there is variation in the motion
230 behavior of the radiosonde. As discussed earlier this may be due to how and when the parachute deployed and if any of the
231 parachute remains entangled with the parachute rigging. The latter is hard to determine without retrieving the radiosonde which
232 is seldom done. We can get a better understanding of the variation in oscillation by looking at individual ascents.

234 Figure 8 and Figure 9 show two descents from Castor Bay Autosonde station (54.50 N, 6.34 W). In both figures panel a shows
235 the processed horizontal wind components u and v components in red and blue respectively. The raw GPS wind components
236 are shown in black and orange for the u and v components respectively. Panel b shows the descent speed and c and d show
237 Lomb periodograms of the detrended raw GPS velocities. In Figure 8 we see that the parachute does not seem to offer
238 significant deceleration to the sonde until about 14 km. here is also descent a weak low frequency oscillations greater than 60
239 seconds over the duration of the descent. In panel figure 8a the raw GPS and the processed v component of the wind track very
240 closely and it is hard to differentiate between them. Figure 9 is a descent from a different day which tells a very different
241 story. The parachute deploys within 1 km of the burst height and causes a sudden deceleration from -60 m s^{-1} to -20 m s^{-1}.
242 After the rapid deceleration the radiosonde enters a high amplitude oscillatory mode with a periodicity of 30-40 seconds as it
243 descends. A hypothesis here is that the sudden deceleration caused by a correct deployment of the parachute has caused the
244 oscillatory mode seen here. The amplitude of oscillations seen under this scenario could introduce error in the processed winds
245 and is a possible area for future study as is the optimal filtering for descent winds.

247 Here it has been shown that identical balloon configurations have very different and random descent characteristics. Figure 3
248 shows that the balloon sometimes twines itself about the parachute which may affect how well the parachute deploys and in
249 turn its oscillatory characteristics on descent. A successful parachute deployment can enhance the oscillation such that it has
250 potential to introduce error in descent wind data, depending on the size of the averaging window used by the sounding software.
251 More research in this area needs undertaking using an approach where motion sensors are attached to the RS41 to better
252 understand the descent to descent variability. Additional investigations where guillotines cut the balloon from the parachute

253 such as that used on heavy scientific balloon payloads, could be utilised to remove the effect of balloon entanglement. The
254 placing of a small central hole in the top of the parachute to improve stability and removal of sudden deceleration also need
255 investigating.
256
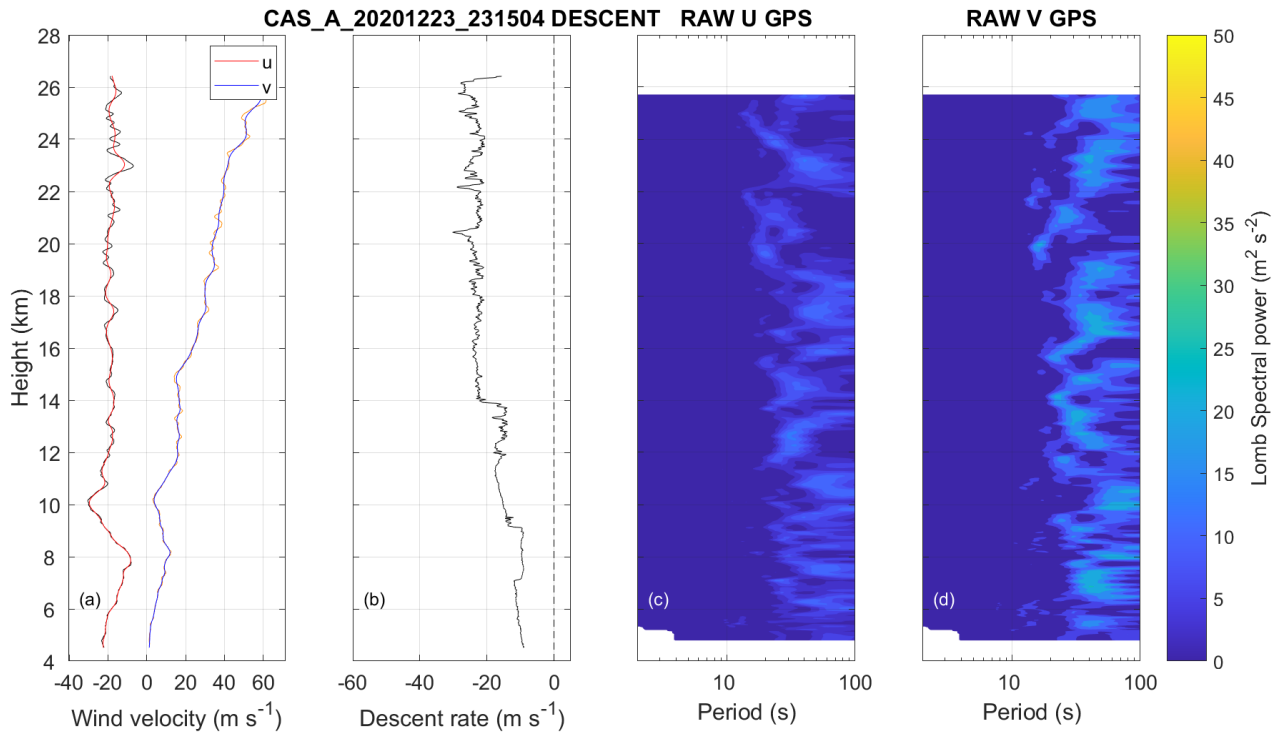
257
258 Figure 8. Vertical profiles of a) processed horizontal wind components *u* and *v* in solid red and blue respectively with raw
259 GPS winds in black and orange for the *u* and *v* components respectively, and b) descent speed. Panels c) and d) show Lomb
260 periodograms of the detrended raw GPS velocities as a function of height for a sounding made at Castor Bay autosonde station
261 (54.50 N, 6.34 W) at 2315UT on 23/12/2020.
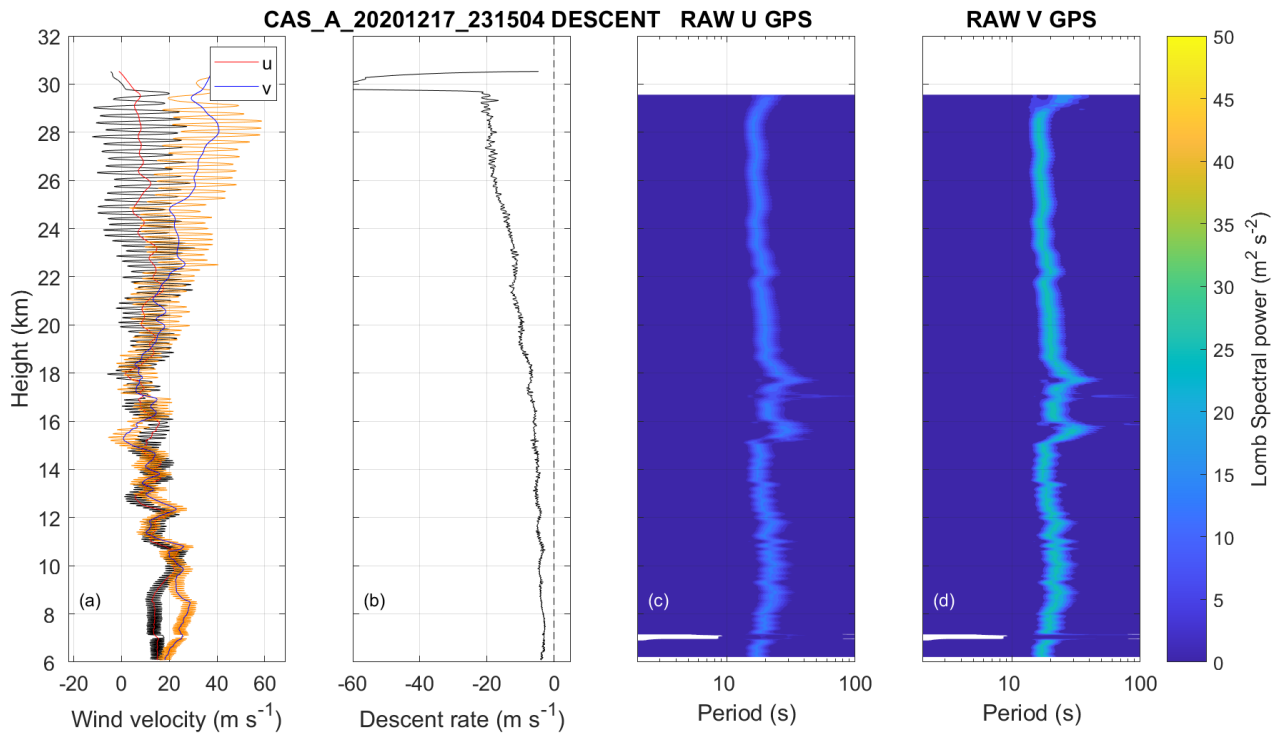
Figure 9. Vertical profiles of a) processed horizontal wind components in solid red and blue for u and v respectively with raw GPS winds in black and orange for u and v respectively, and b) descent speed. Panels c) and d) show Lomb periodograms of the detrended raw GPS velocities as a function of height for a sounding made at Castor Bay Autosonde station (54.50 N, 6.34 W) at 2315 UTC on 17/12/2020.

In summary, ascending radiosondes tend to have similar characteristics in terms of motion beneath the balloon and ascent speeds, although the latter does depend on the amount of gas within the balloon. Descending radiosondes have widely varying descent characteristics which are due to the random nature of how the balloon and parachute interact (if present) and how effective the parachute is at slowing the balloon. The motion on descent may be more consistent if the radiosonde could be 'cut free' of the balloon remains and fall on its own without a parachute. It would be interesting to study the effect of cutting the string just after balloon burst, but this may be technically difficult and the risk associated with the radiosonde falling at terminal velocity would need to be assessed. Given the variation in burst heights, reliably cutting it before burst would reduce the average height attained. In addition similar motion and orientation sensors as used in Harrison & Hogan (2004) and Marlton et al. 2015 could be used to ascertain more information about the orientation of the descending radiosonde package

16

3 Comparison with ECMWF background fields

3.1 ECMWF forecasting system

For comparison we use statistics from the ECMWF operational data assimilation system for September to November 2019. The forecast model had a horizontal grid spacing of about 9 km and 137 levels in the vertical and the assimilation used 4DVar with a 12 h window. The 3...15 h forecast from the previous analysis forms the background for the assimilation and the observation-minus-background (O-B) statistics can yield a lot of information. The background values are not perfect but provide a relatively accurate and (generally) independent estimate of the measured variables. In many respects the forecasting system is similar to that of ERA5 (Hersbach et al, 2020) which was based on the operational system of 2016. One difference from ERA5 is that treatment of radiosonde drift was introduced operationally in June 2018 and this improved upper-level O-B standard deviations by 5-10% (Ingleby et al, 2018). Prior to this radiosonde profiles were treated as vertical and instantaneous. Afterwards, and in this study, ascent profiles were split into sub-profiles of 15-minutes each and treated as valid at the time and latitude/longitude of the first point in the sub-profile. Descent profiles are split into 5-minute sub-profiles for comparison with the model.

3.2 Wind comparison

Figure 10 shows mean and standard deviation (SD) profiles of O-B differences at radiosonde standard levels for the u (zonal) component of the wind. The statistics for the v (meridional) component are similar and are not shown. The mean differences (dashed lines) are close to zero, as hoped. The standard deviations are approximately 2 m s^{-1}, but are slightly larger at the top levels. One surprise was that the descent profiles (in red) fit the variations in background wind more closely than the ascent profiles (in black), particularly at upper levels. Comparing individual ascent/descent profiles the descent winds generally appear smoother and this appears to be the cause of the better fit to background. This is illustrated in Figure 11 which shows the raw 1-second data for a single profile (faint line) and the data after smoothing to remove the pendulum motion (bold line). In this case the smoothing was performed using the GRUAN algorithm (Dirksen et al, 2014), whereas the BUFR reports have smoothing applied by Vaisala MW41 software which is similar but not identical. In both cases a time filter with a fixed window is applied to all profile data. Improvements to this are possible as is clear from Section 2.5. Because the radiosonde is falling faster than it ascended, a filter based on a fixed time interval corresponds to a larger height interval on the descent. Note also that the MW41 processing does not include an inertial correction as used in the AVAPS dropsonde processing (Sect. 1), which would counteract time-lag effects - largest when falling fastest. As shown in Figure 11 (also S6 and S7 in supplement), at most levels there is less high frequency 'pendulum' motion on the descent - although at the top levels there can be substantial amounts of noise.

Figure 12 shows SD(O-B) for individual descents in the interval 30-50 hPa against the mean descent rate for this pressure range. The standard deviations are slightly larger for slower descent rates, this is thought to be linked to larger amplitude

309   pendulum motion when the parachute is slowing the descent more effectively. Similar effects can be seen for other pressure
310   ranges, but there is no clear dependence of the mean (O-B) winds on descent rate (not shown).
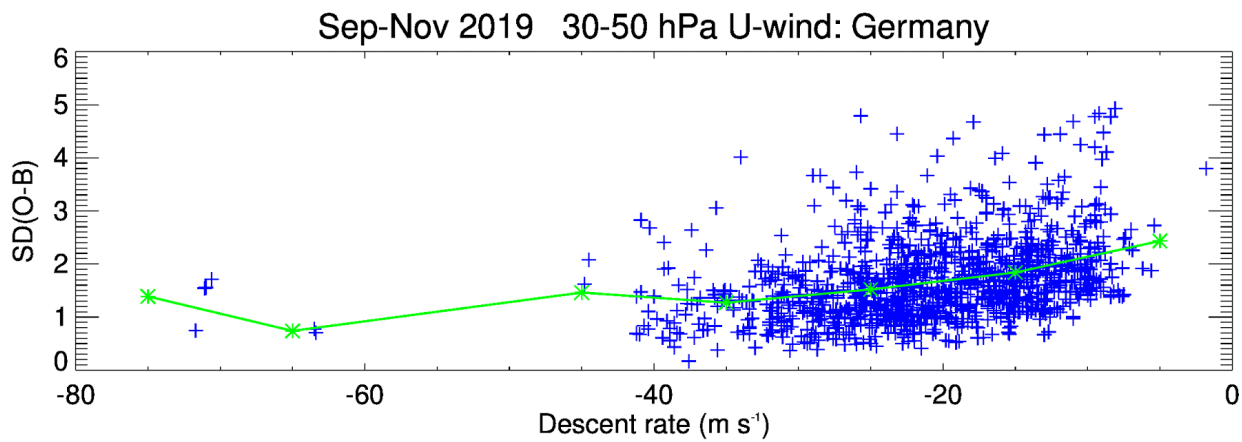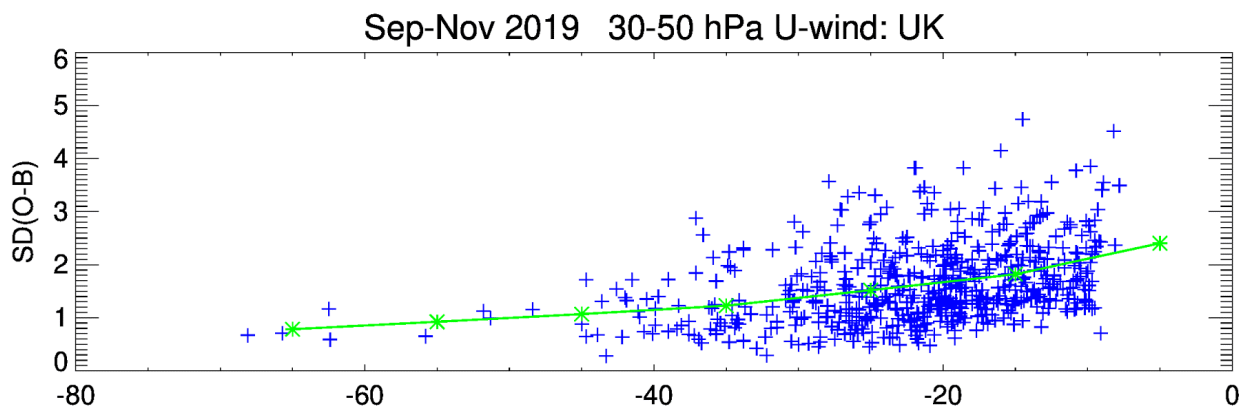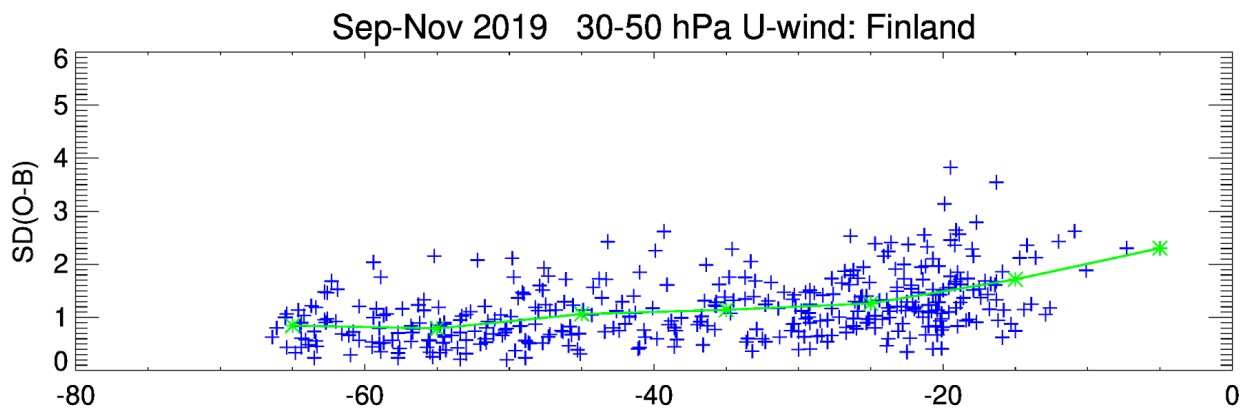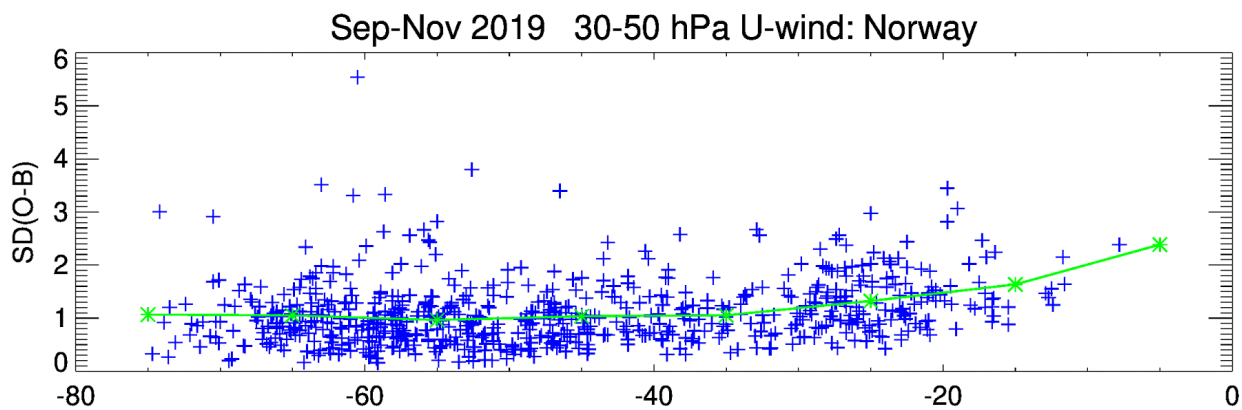

311
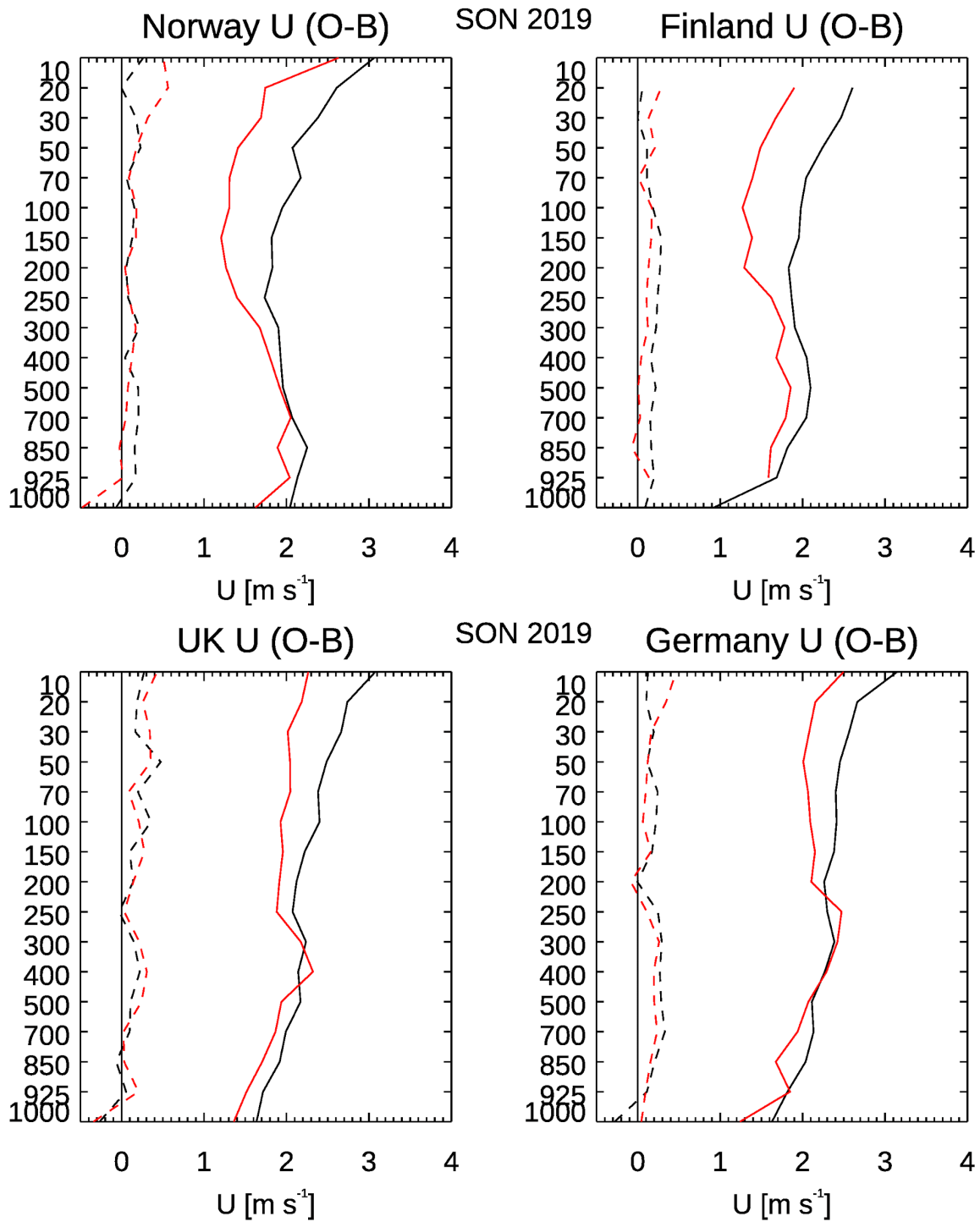
Figure 10. U-component standard level statistics of mean (dashed) and SD (solid) O-B differences for ascent (black) and
313 descent (red) for four different countries, September - November 2019.
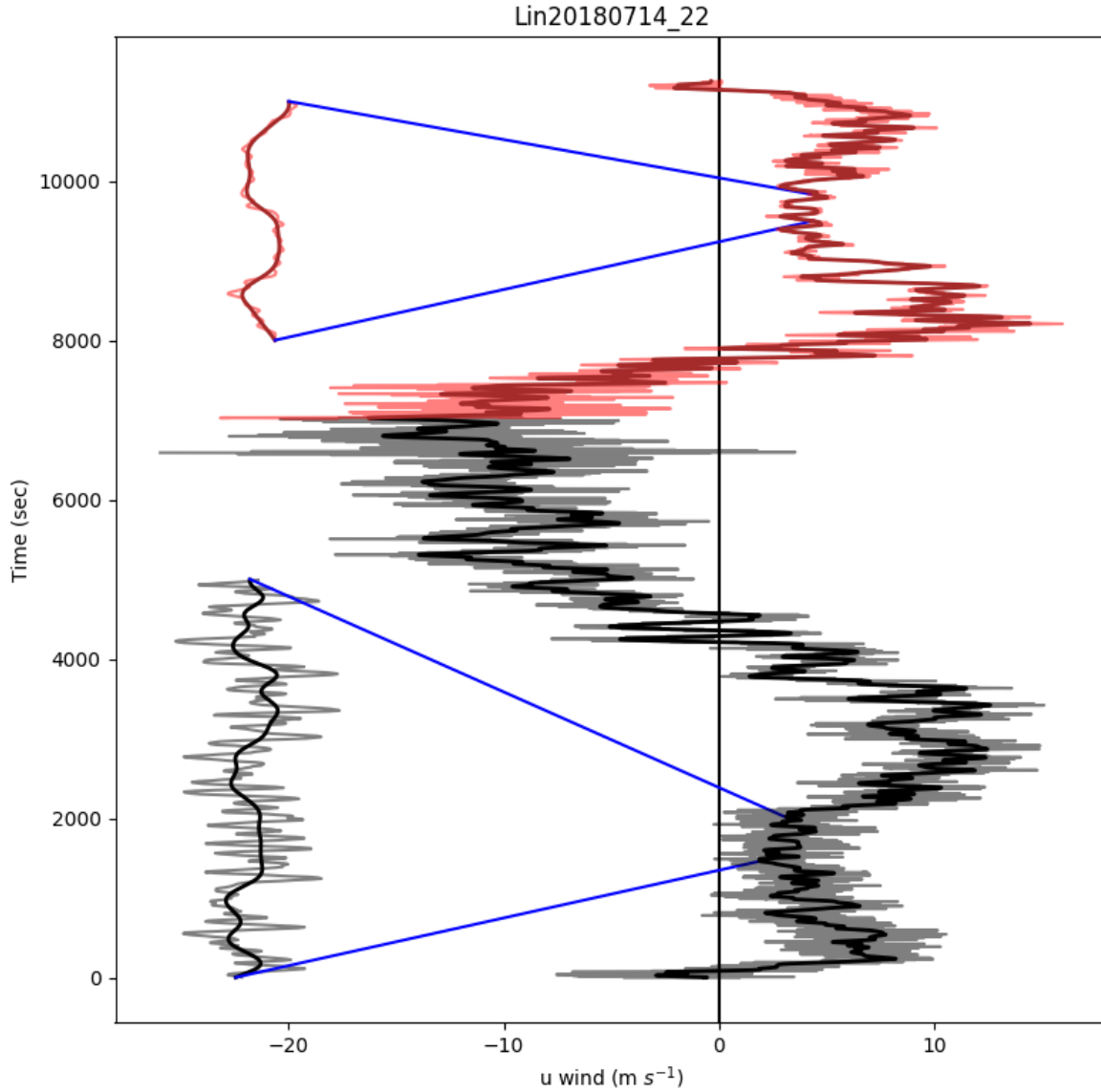
Figure 11. Raw (1-second) data (pale line) and filtered (bold line) u component as a function of time: ascent (black) and descent (red). This is for a launch from Lindenberg, including a parachute for the descent. Two sections have been shown in more detail with the time axis scaled by 10.

Sep-Nov 2019   30-50 hPa U-wind: Norway

Sep-Nov 2019   30-50 hPa U-wind: Finland

Sep-Nov 2019   30-50 hPa U-wind: UK

Sep-Nov 2019   30-50 hPa U-wind: Germany

Descent rate (m s^{-1})

319 Figure 12 Standard deviation of (O-B) plotted against mean descent rate, both for descents from 30 to 50 hPa (blue symbols).
320 The green symbols show average values for bins of 10 m s-1.

321 **3.3 Temperature comparison**

322 Firstly, we note that at about 50 hPa, in the extratropics, the ECMWF background is too cool by about 0.5°C (this can be seen
323 against the RS41 ascent data in Figure 13). This is recognised as a model error, due mainly to excessive humidity and hence
324 extra long-wave cooling as shown by Shepherd et al (2018). More recent work on the analysis system has approximately
325 halved the short-range forecast bias (Laloyaux et al., 2020); they included comparison against radio occultation (RO) retrievals.
326 We compared radiosonde ascent/descent pairs with RO retrievals that were within 100 km and 2 hours of the burst point. The
327 RO data is much closer to the ascent temperatures than the descent temperatures - note that the sample size is much smaller
328 than for the O-B statistics (137 versus 2190 at 70 hPa).

329

| Pressure (hPa)	Sample	Ascent-RO (°C)	Descent-RO (°C)	Ascent-B (°C)	Descent-B (°C)
5	22	-0.07	1.07	-0.37	0.90
10	36	0.53	1.63	0.25	1.25
20	125	0.13	1.04	0.37	1.33
30	130	0.15	0.92	0.45	1.24
50	135	0.02	0.37	0.44	0.84
70	137	-0.11	0.17	0.39	0.68
100	136	0.28	0.41	0.31	0.51

330

331 Table 2. Collocations with radio occultation retrievals (within 100 km and 2 hours) for all stations at standard levels, with
332 mean temperature differences (°C). Columns show Radiosonde Ascent (or Descent) minus RO or Background values, the
333 comparisons with the background are limited to the profiles collocated with RO.

334

335 The clearest difference between ascent and descent is that at upper levels the descent temperatures are higher than the ascent
336 values (Figure 13). This has been noted previously, for different radiosonde types, see section 1. At 10 hPa the descent-ascent
337 difference is over 1.5°C for the Norwegian stations and about half that for the UK and German stations. For Finland the
338 highest standard level reached is generally 20 hPa and the difference there is about 1°C. One hypothesis advanced was that
339 this could be a time-lag effect. The temperature sensor response time at 6 m s^{-1} flow is 0.5 s at 1000 hPa, 1.2 s at 100 hPa and
340 2.5 s at 10 hPa (Vaisala, 2017b). (For higher flow speed the response time is shorter. RS41 temperature data is time-lag
341 corrected both in ascent and descent phases.) However, descending from 30 to 100 hPa the mean temperatures over Northern
342 Europe were approximately constant or increasing slightly (not shown) suggesting that another explanation is needed. A
343 convincing link to the radiosonde fall speed was found (Figure 14). There is no clear link to the time of day (and solar radiation)
344 as shown by the different coloured symbols in Figure 14. The SD(O-B) for temperature shows no clear link to fall rate (not
345 shown).

346 Returning to Figure 13 the large top-level ascent-descent difference in the Norwegian data disappears below 300 hPa, but the
347 smaller top-level Finnish difference becomes an offset of 0.2 or 0.3°C throughout the troposphere. The important difference
348 seems to be that the Norwegian radiosondes have a pressure sensor, but the Finnish radiosondes do not. Without a pressure
349 sensor the pressures must be computed and biases in the temperature will feed into later biases in the pressures - discussed in
350 more detail in the next section. A smaller version of the same effect can be seen between the German data (with pressure
351 sensors) and the UK data - without a pressure sensor these have an offset of about 0.1°C in the troposphere: smaller than the
352 Finnish data because the UK radiosondes have parachutes.
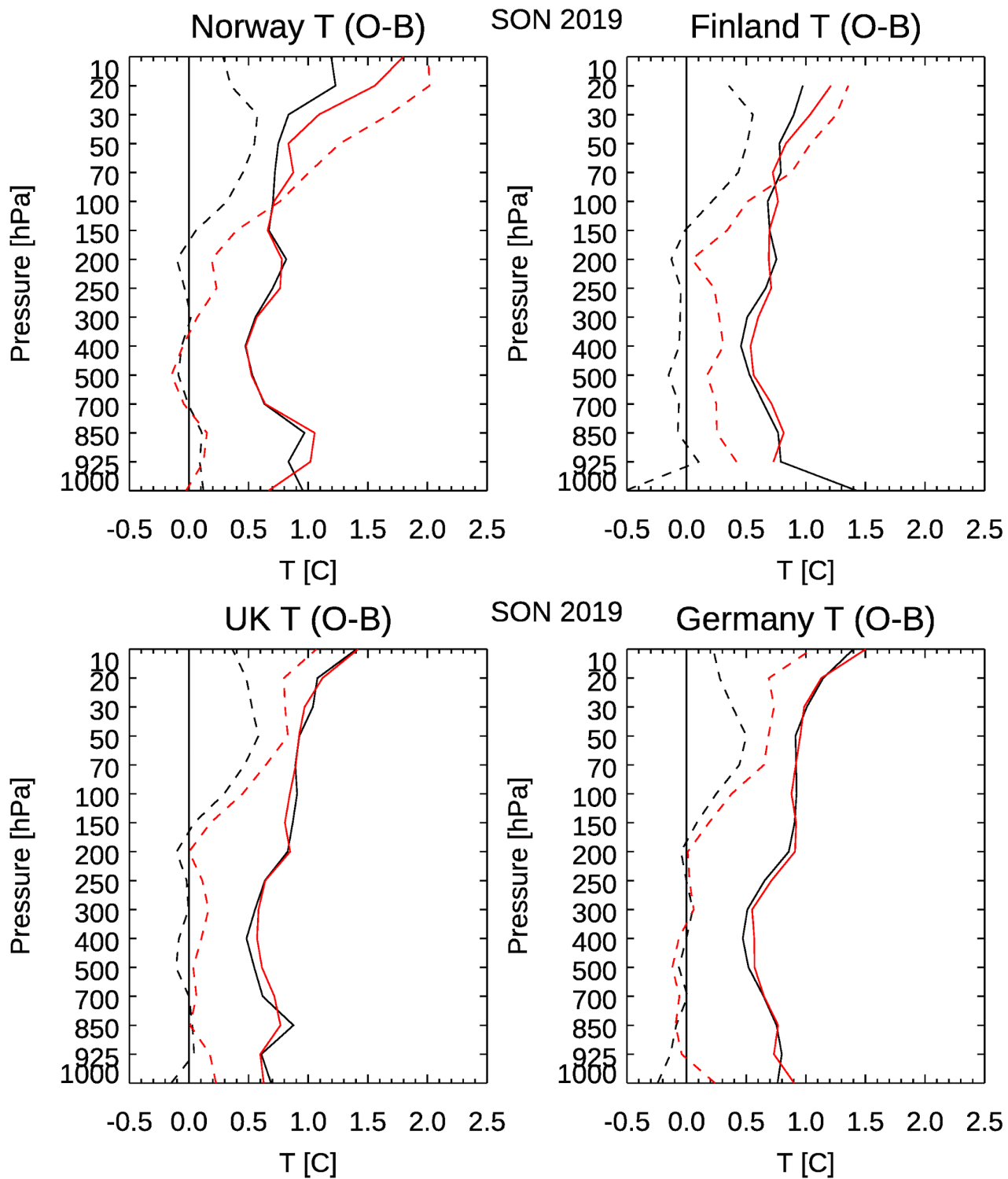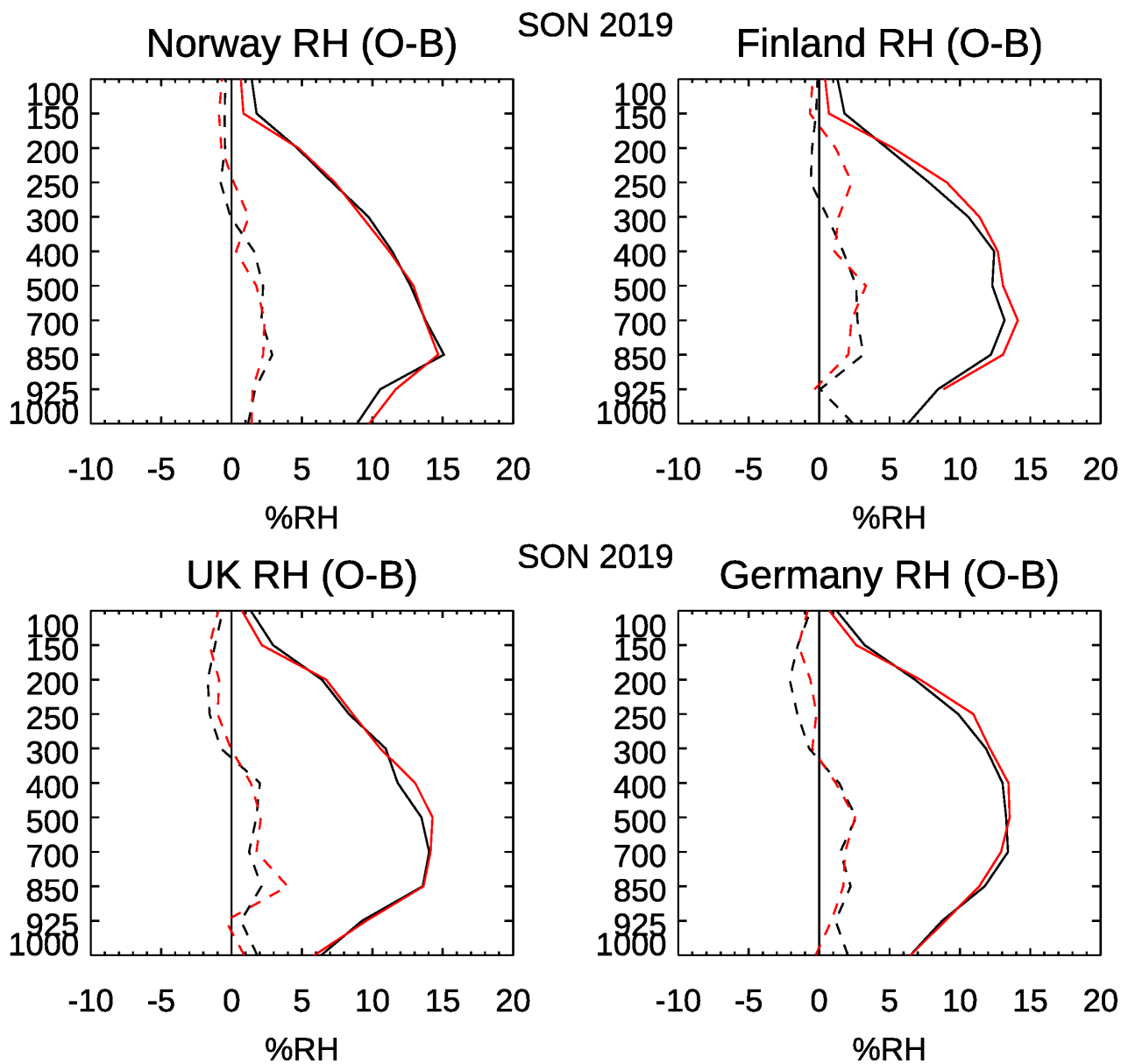
Figure 13. As figure 10 but for temperature.
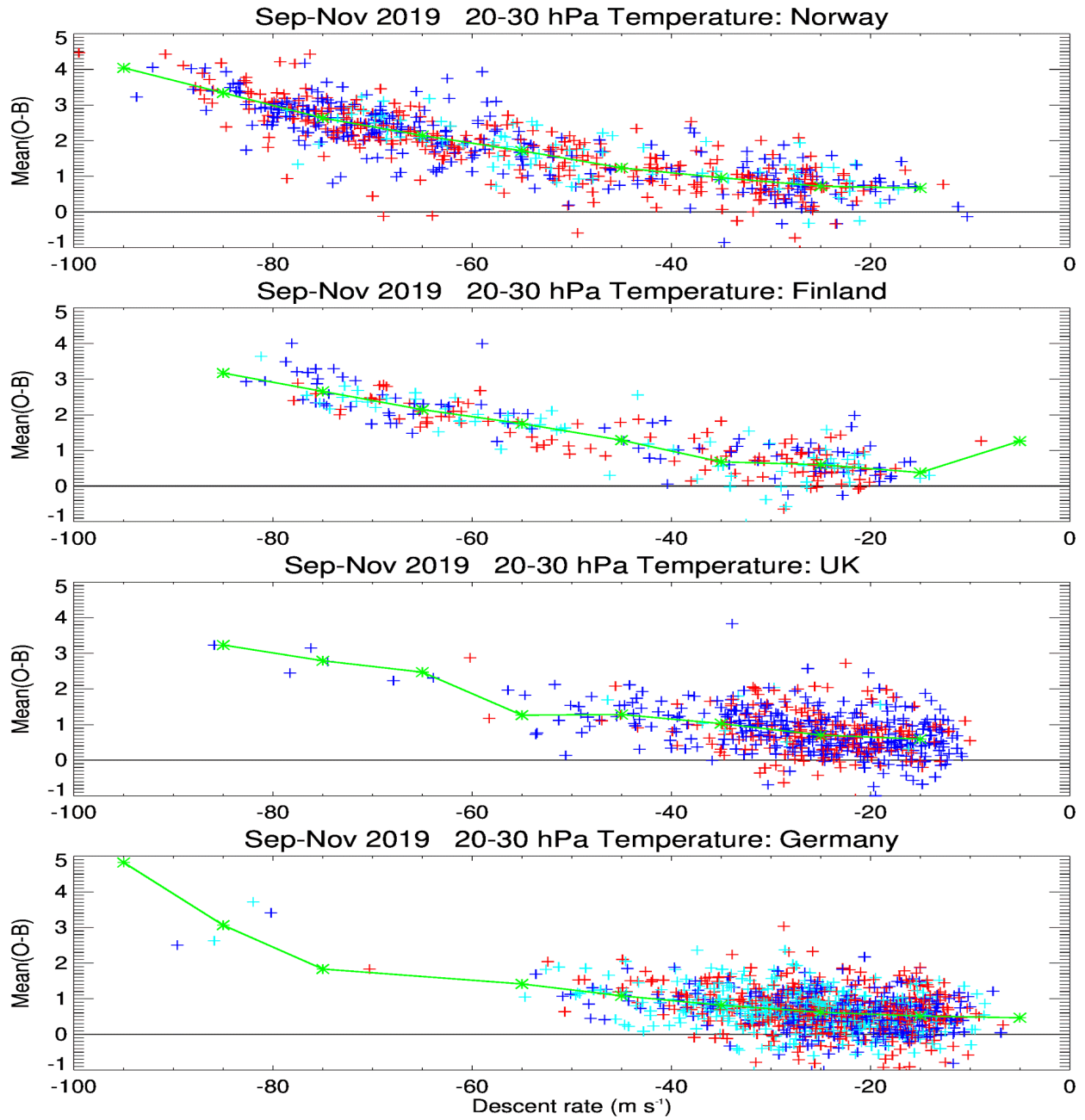
Figure 14. Comparison between mean fall speed from 20 to 30 hPa and mean O-B temperature. Red markers denote nominal 12 UTC profiles, dark blue markers nominal 00 UTC profiles and cyan denotes intermediate profiles. (Recall that the B values have a bias of about 0.4°C at these levels.)   Green markers show values averaged over all times of day in bins of 10 m s^{-1}.

356

357

358

359

360

3.4 Humidity comparison

Figure 15 shows ascent/descent comparisons with the background for relative humidity (RH) (see supplement for specific humidity). Broadly speaking the ascent and descent statistics are very similar, although the descent fit to background is slightly worse for the Finnish radiosondes in the troposphere. Between about 50 and 150 hPa the SD(O-B) for RH is smaller for the descent, but note that stratospheric radiosonde humidity is not assimilated in the ECMWF or other NWP systems.

366

Figure 15. As figure 10 but for relative humidity - up to 100 hPa.

4 Warm bias during descent

4.1 Direct effect of heating

As the comparison of descent data with NWP model suggests, there is a positive temperature bias in the data measured by descending Vaisala RS41 radiosondes. This bias is bigger in the stratosphere than in the troposphere and is more significant for the data taken from radiosondes without parachutes.

As the descent rate often exceeds 50 m s^{-1}, occasionally even 100 m s^{-1}, frictional heating seems to be a reasonable explanation of the observed bias. A related issue is recognized for sensors on aircraft, which also measure temperature while moving fast relative to the free air (WMO 2018b, section 3.3). For aircraft the kinetic energy is transferred to internal heat mostly by adiabatic compression. For radiosondes we expect that most of the conversion is done by direct collisions of air and sensor molecules (friction), but it is also possible that the effect is done by adiabatic compression in the boundary layer of the sensor. We use a quadratic relationship on descent rate (DR) - this arises from a simple energy balance, independent of the energy conversion mechanism:

$$\Delta T = A.DR^2 \quad (2)$$

A is a coefficient, determined below. This is similar to the equation for the heating of aircraft temperature sensors - see Appendix. It is also linked to the 'viscous dissipation' or 'compressional heating' mentioned by Wagner (1964) for rocketsondes (launched high in the atmosphere by a rocket they measure on the descent, slowed by a parachute). This relationship was examined by comparing the descent temperatures with ascent temperatures from the same radiosonde. Most of the data were from the Praha-Libus (Prague) upper air station: three launches per day, 554 descents with average length of descent 23 km; there were about 528 000 points at which ascent and descent could be compared. The data covers the period from July 2019 to January 2020, using RS41-SG radiosondes without pressure sensor or parachute (as for the Finnish soundings above).

The time and space difference between ascent and descent at a particular level is zero at balloon burst and can rise to 2 hours and 150 km for lower tropospheric levels. This difference will result in deviations of atmospheric measurements. In section 3 the model values (including model diurnal cycle) are subtracted from the radiosonde temperatures, but comparing ascent and descent directly samples the diurnal cycle. There is little diurnal cycle at upper levels but below 4 km we expect to see mean descent-ascent differences due to the diurnal variation and time difference.

For each point we have height (H), descent rate (DR) and descent temperature (T_D), with ascent temperature (T_A) interpolated to this level. After dividing the sample into bins of 1000 m in altitude the bias was calculated (mean temperature difference $\Delta T = T_D - T_A$) for each bin. Results shown in Figure 16 are very similar to comparison of German data shown in Figure 13 – about 1°C bias at the highest levels decreasing to 0°C at 12 km. The low-level descent-ascent differences are -0.4°C, 0.2°C and 1.1°C for the 00, 06 and 12 UTC profiles respectively, reflecting the diurnal cycle and giving a positive bias overall.

According to equation [2], ΔT should depend solely on DR. Pearson's correlation coefficients confirms the strong link between those two variables. It was 0.21 between ΔT and H, between ΔT and DR it was 0.40.
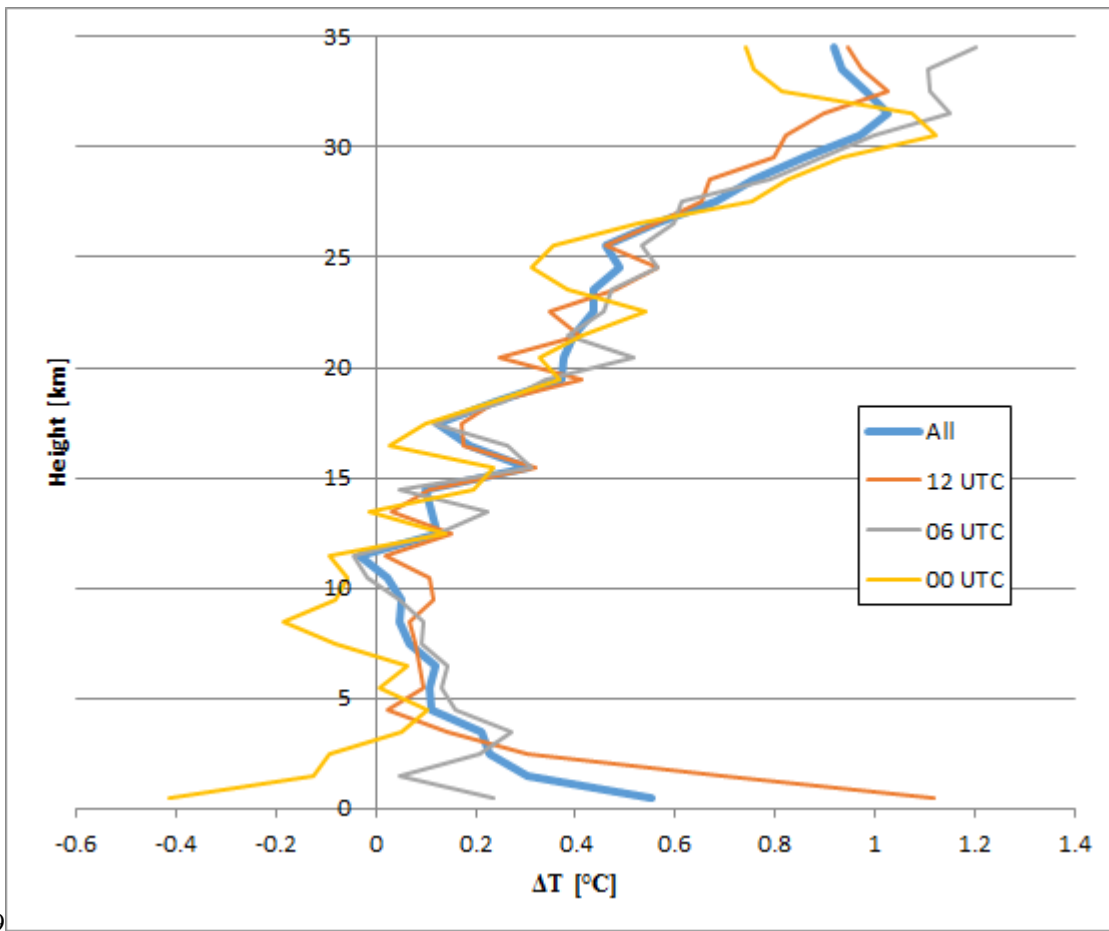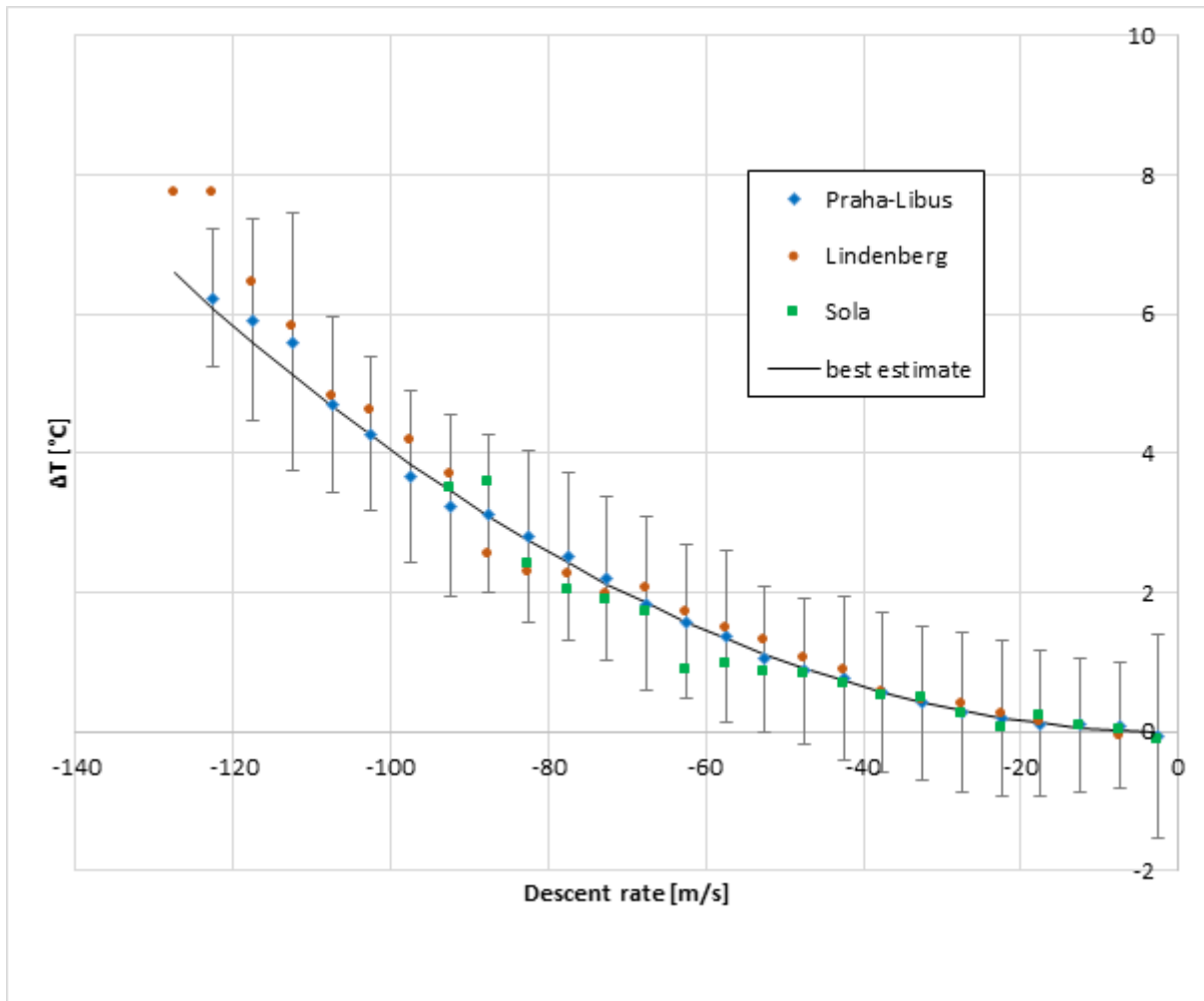
Figure 16. Temperature differences between ascent and descent as a function of height (Praha-Libus data).

In the next step the sample was binned by DR – intervals used were 0-5 m/s, 5-10 m/s etc. There is clearly a quadratic dependence of ΔT on DR in Figure 17 (average ΔT for these bins). The standard deviation of ΔT shown with grey lines is almost independent of DR. The black line is the best estimate with $A = 4.05 \cdot 10^{-4}$.

For DR greater than 110 m/s the fit is slightly less good but the sample size is small with data available from less than 3 % of examined soundings. When equation [2] with $A = 4.05 \cdot 10^{-4}$ is applied as a temperature correction, the root mean square ΔT is lowered from 1.22 °C to 1.06 °C, indicating that the correction explains 24.4 % of the variance seen.

Calculating the correction as a complete quadratic equation ($\Delta T = 4.39 \cdot 10^{-4} \cdot DR^2 - 3.17 \cdot 10^{-3} \cdot DR + 5.40 \cdot 10^{-2}$), did not significantly improve the result (explained variance increased by less than 0.01 %).

To find out if the result was affected by lower tropospheric differences (which are mostly caused by diurnal variation and not friction), the result was recalculated for the sample with all data below 4 km excluded. Results changed only very slightly again, the coefficient was then $A = 4.04 \cdot 10^{-4}$, and the explained variance increased to 25.3 %.

28

417

418
419 Figure 17. Dependence of temperature differences between ascent and descent on descent rate, Praha-Libus, Lindenberg and
420 Sola averaged over different times. For Praha-Libus the standard deviation and best estimate are shown.
421

422 The coefficients were also calculated separately for the data from each time of the launch
423 − 00, 06 and 12 UTC soundings − the estimates of coefficient A range from $3.9 \cdot 10^{-4}$ to $4.3 \cdot 10^{-4}$
424 (Table 3).

| Best estimate (at time, UTC) $\Delta T = A \cdot DR^2$	A $[°C \cdot s^2 \cdot m^{-2}]$
00	$3.90 \cdot 10^{-4}$
06	$4.22 \cdot 10^{-4}$

29

12	$4.07 \cdot 10^{-4}$

Table 3. Best estimate of correction coefficient for different times of launch at Praha-Libus.

Figure 18 shows the mean and SD of ΔT as a function of height before and after applying the correction. We can see that bias was almost completely removed, except for the lowest layers, where the bias is expected due to diurnal effects. Another notable result was that ΔT SD for heights above 20 km was significantly lowered.
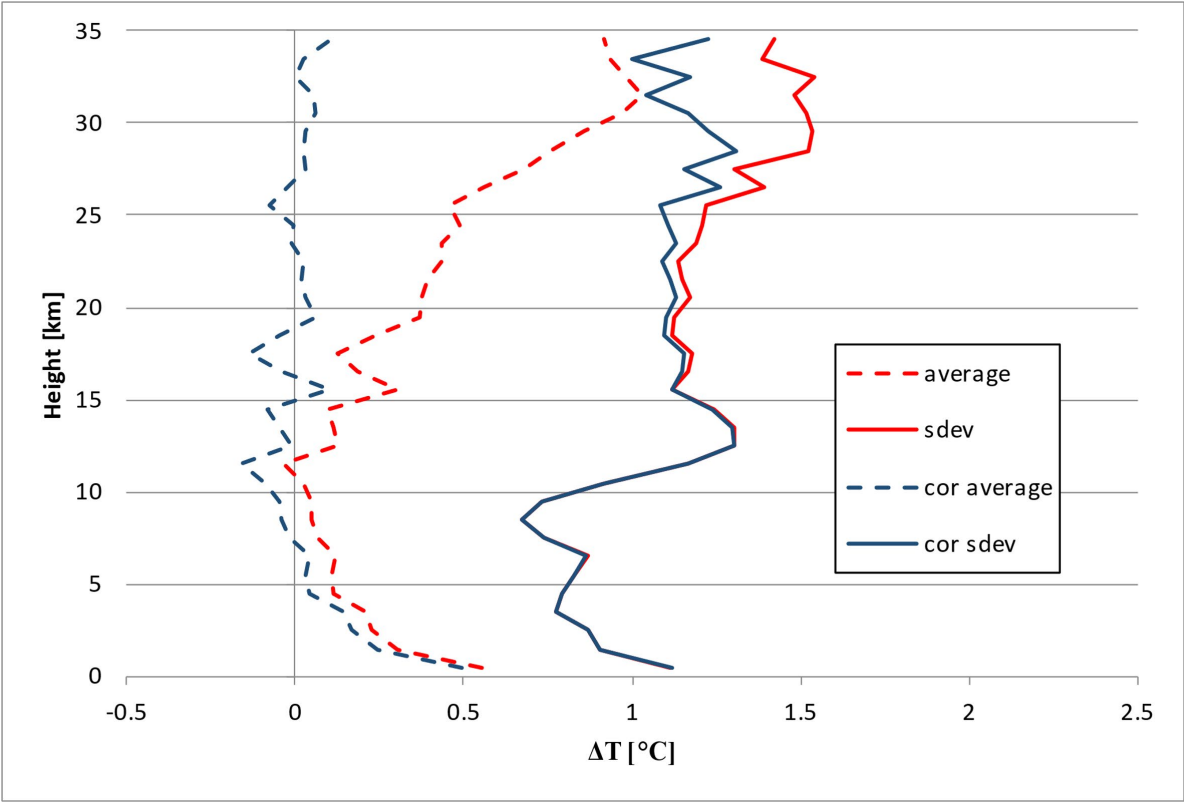
Figure 18. Average ΔT and its standard deviation before and after friction correction (Praha-Libus).

Investigations were extended to other stations to examine consistency. Information about type of the data, data sample and calculated coefficient are in Table 4.
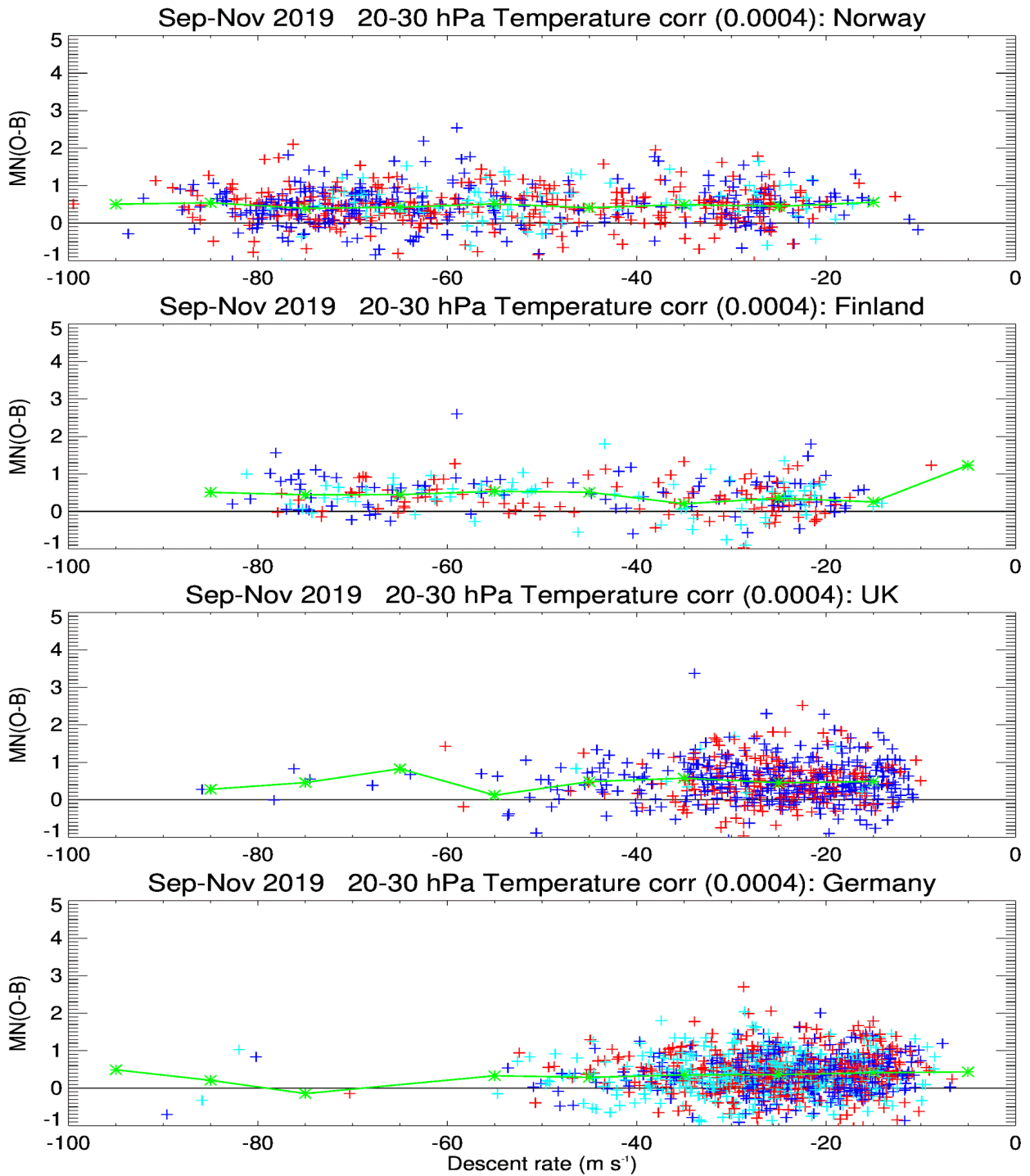
Station	Praha-Libus	Lindenberg	Sola

Country	Czechia	Germany	Norway
Radiosonde	RS41-SG	RS41-SGP	RS41-SGP
Parachute	no	yes	no
Sample start	Jul 2019	Nov 2019	Dec 2019
Sample end	Jan 2020	Feb 2020	Jan 2020
Soundings	554	329	45
Sample size	527 779	650 399	37 670
Coefficient A	$4.05 \cdot 10^{-4}$	$4.46 \cdot 10^{-4}$	$3.44 \cdot 10^{-4}$

440   Table 4: Coefficient A determined from different samples

441

442   It can be seen from the results in Table 4 that the exact value of the correction coefficient is slightly uncertain. To check with

443   a larger sample Figure 19 shows the differences from ECMWF background for the 20 to 30 hPa layer but with the descent

444   temperatures adjusted using $A = 4 \cdot 10^{-4}$, This does a good job of removing the speed dependent biases seen in Figure 14 (the

445   correction also works well at other stratospheric levels). This suggests that it may be sufficient to have the same correction

446   applied with and without a parachute.

Sep-Nov 2019   20-30 hPa Temperature corr (0.0004): Norway

Sep-Nov 2019   20-30 hPa Temperature corr (0.0004): Finland

Sep-Nov 2019   20-30 hPa Temperature corr (0.0004): UK

Sep-Nov 2019   20-30 hPa Temperature corr (0.0004): Germany

Descent rate (m s^{-1})

447

32

Figure 19. Comparison between mean fall speed from 20 to 30 hPa and mean O-B temperature after correction using A=0.0004 (cf Figure 14). Green markers show values averaged over all times of day in bins of 10 m s^{-1}.

4.2 Indirect effect of heating

Some radiosondes, including the RS41-SGP, measure atmospheric pressure directly and the geopotential height is calculated using the hydrostatic equation: $dP = -\rho(H) g \, dH$, where the density of air ρ depends on pressure, temperature and humidity. The RS41-SG radiosonde measures geometric height using GPS, this is converted to geopotential height, and the pressure is calculated with the hydrostatic equation.

As discussed above, descent at high speeds, mostly in the stratosphere, causes the measured temperature to be too high. This overestimation of temperature leads to underestimation of air density. For the RS41-SGP it means that (negative) height increments are smaller than they should be and thus for the certain pressure level, higher altitudes are reported than they should be. As the height errors accumulate during the descent, the shift of height affects the troposphere levels, where direct heating impact is negligible. For RS41-SG radiosondes, the effect is similar, resulting in an underestimation of pressure increments, causing a lower pressure for a given height - illustrated in Figure 20.

The shift of the profile is visible only if we use as a vertical coordinate the variable which is calculated, not directly measured. As most applications (including many NWP systems) use pressure as vertical coordinate, the effect can be seen for RS41-SG radiosondes. It should lead to an increase in SD when comparing variables to the NWP model, but also to increase of tropospheric temperature bias due to the temperature gradient in the troposphere (as can be seen in Finnish data compared to ECMWF in Figure 13).

The effect is clearly visible in Figure 21. For the Praha-Libus data sample ascent and descent levels were matched both using height and using pressure. In the stratosphere the choice of coordinate has little impact on the ΔT statistics (because ΔT comes mainly from direct heating). In the troposphere, the friction is much lower due to the slower DR and for pressure-matched levels, the shift of the profile caused by accumulated pressure errors is responsible for most of the bias. Up to 11 km there is also visible worsening of SD for pressure-matched profiles due to this effect.
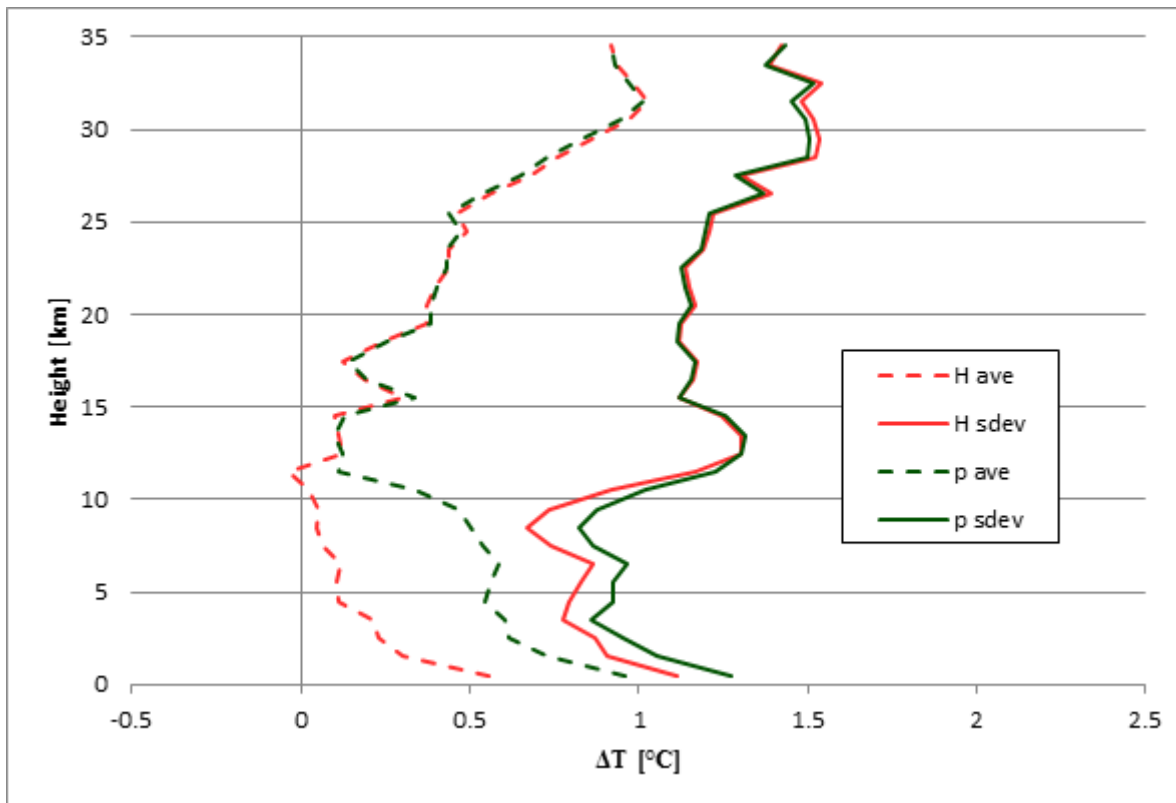
33
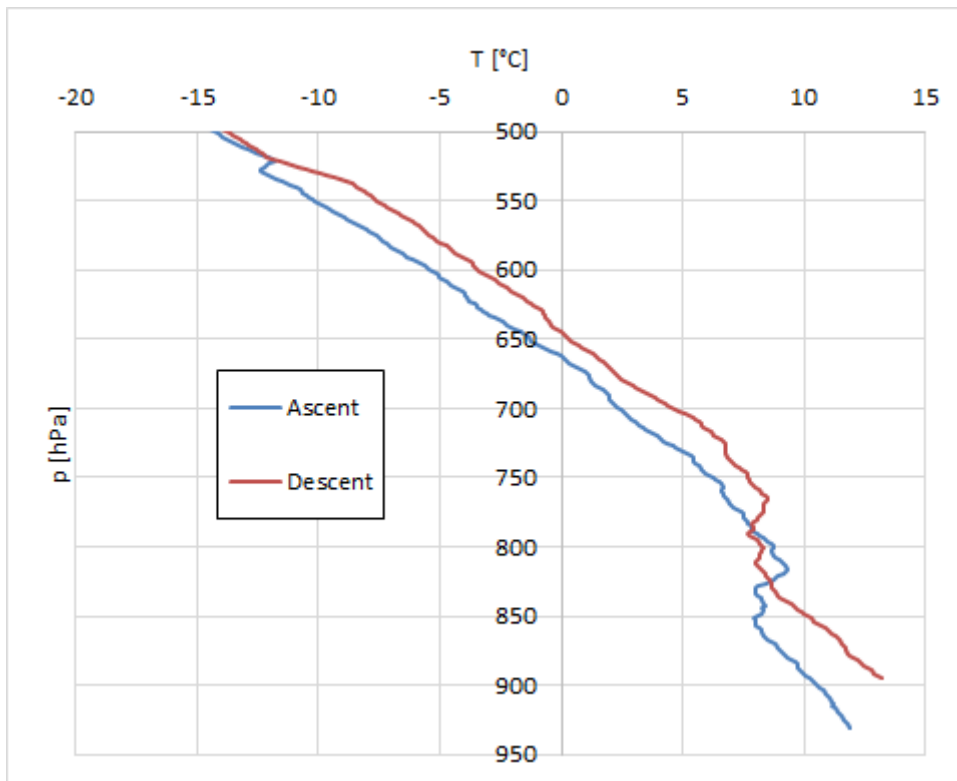
471

472   Figure 20: Shift of the tropospheric profile as a function of pressure. Profile from 23-09-2019, 12 UTC, Praha-Libus.

473

Figure 21: T bias and SD when ascent/descent matched using height (red) or matched using pressure (green), averaged over seven months of Praha-Libus profiles.

The improvement of pressure differences after application of the temperature correction, Eq (2), and recalculating pressure using corrected temperature is clearly visible in Figure 22. The recalculation was made on a data sample from Praha-Libus, and the pressure bias near the surface was decreased by approximately 95 %.
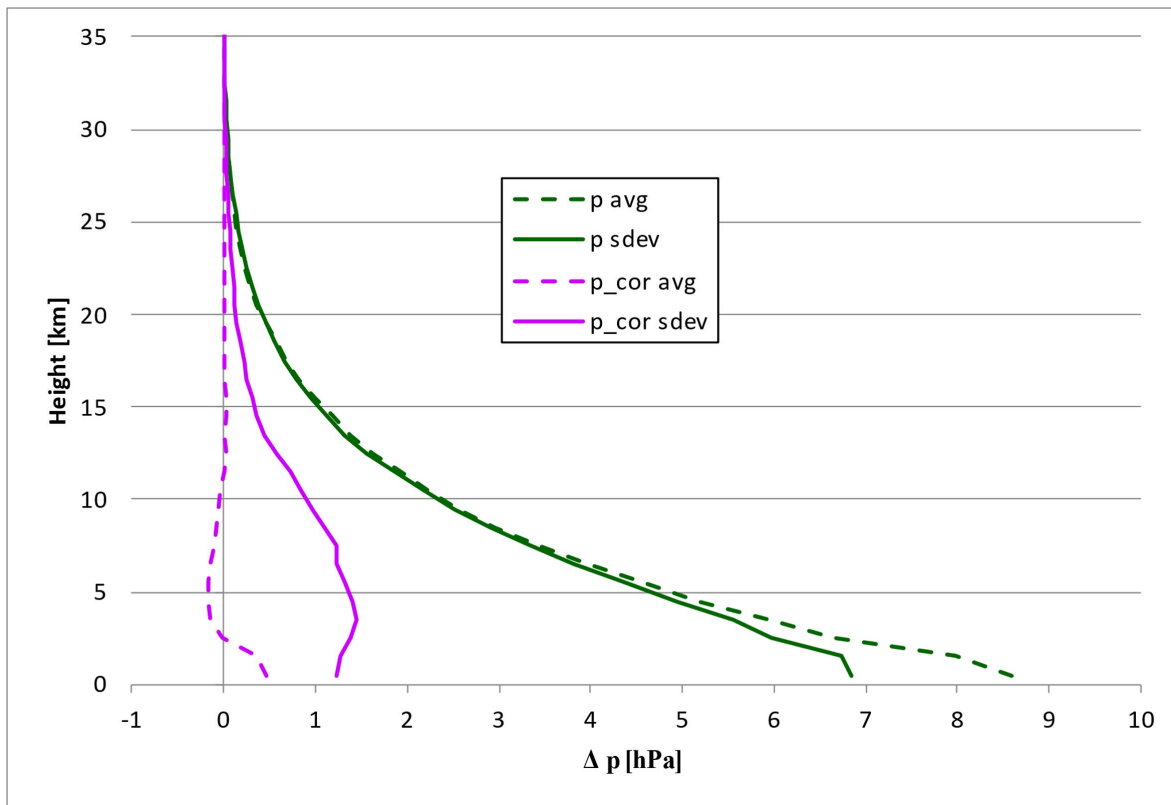
Figure 22: Average Δp (=p_{ascent} - $p_{descent}$) and its standard deviation before and after applying temperature correction for friction and pressure recalculation.

Figure 23 shows the bias (dashed) and SD (solid) relative to the ascent for two versions of Praha-Libus temperature descent data (all the data used T_{cor} according to Eq. (2)); data were matched by pressure either reported or recalculated using the corrected temperature. The negative effect of accumulated pressure error due to friction (green line) was removed by the pressure correction. The corrected (purple) lines on figure 23 are almost identical with the red lines on figure 21 using data matched by height. Thus the pressure errors arising from stratospheric heating of the temperature sensor can largely be removed by using corrected temperatures in the hydrostatic calculations.
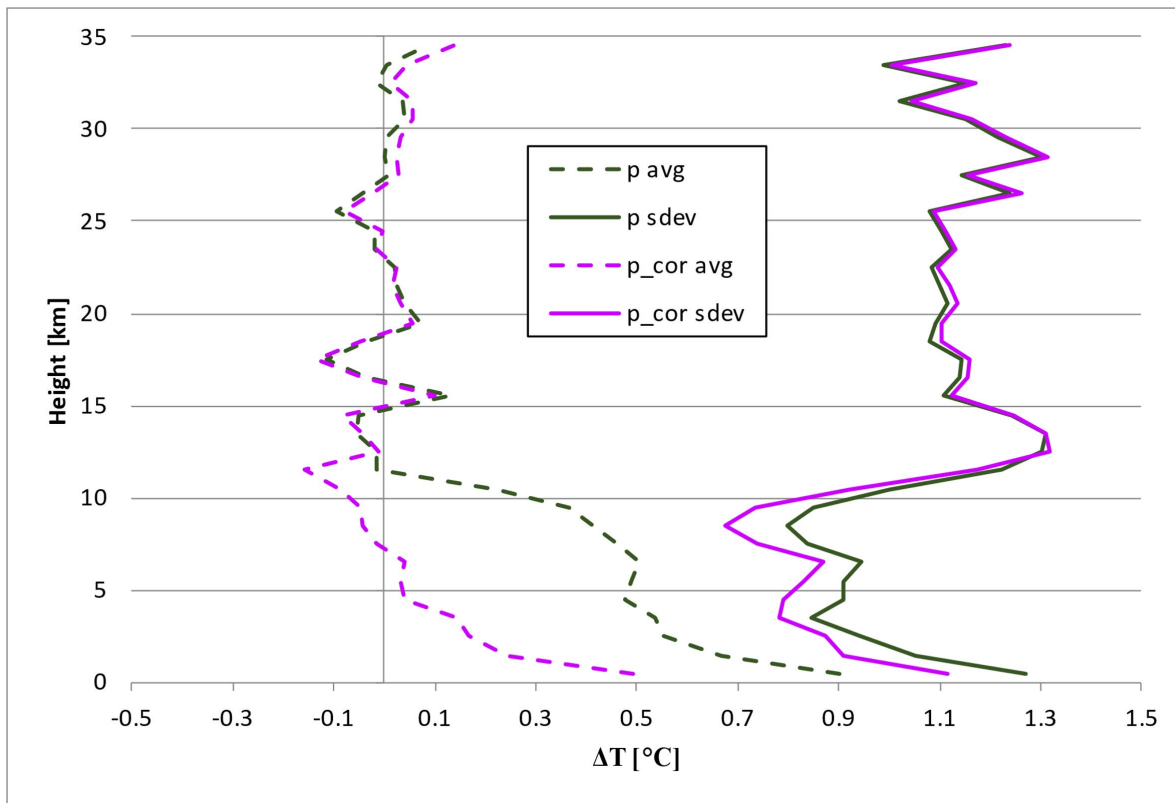
Figure 23: Temperature bias and SD between ascent and descent matched using either reported pressure (green) or corrected pressure (purple). Accumulated Praha-Libus data, the friction correction was applied to all temperatures.

5 Assimilation of descent data

Partly prompted by the drop in numbers of aircraft data due to the Covid-19 pandemic (Ingleby et al, 2021) a trial was run assimilating European RS41 descent data for 20 January to 28 April 2020. The large-scale impact was very small as expected, but over Europe there were modest improvements in the root-mean-square (rms) fit of the 12 h forecast to radiosonde ascent data (Figure 24 100*rms_test/rms_control is shown). There were improvements over Germany (not shown) and the impact was mixed over Scandinavia. The decision was taken to assimilate only the German descent data for the time being - this is the best subset, because they have parachutes and pressure sensors, as discussed in section 3 - implemented operationally on 17 June 2020. Upper-level temperatures were excluded because of the biases. Upper-level winds were used in the trial, but because of concerns about accuracy when the radiosonde is falling fast all descent data with pressure less than 150 hPa are excluded in the current operational system. Note that at the upper-levels the ascent and descent are close together in space and time and so one may not want to assimilate both ascent and descent profiles. As discussed in section 4, some of the bias

37

507   problems would be reduced if height was used as the vertical coordinate rather than pressure - however this would involve

508   significant work and testing, so there are no plans to do so in the near future.
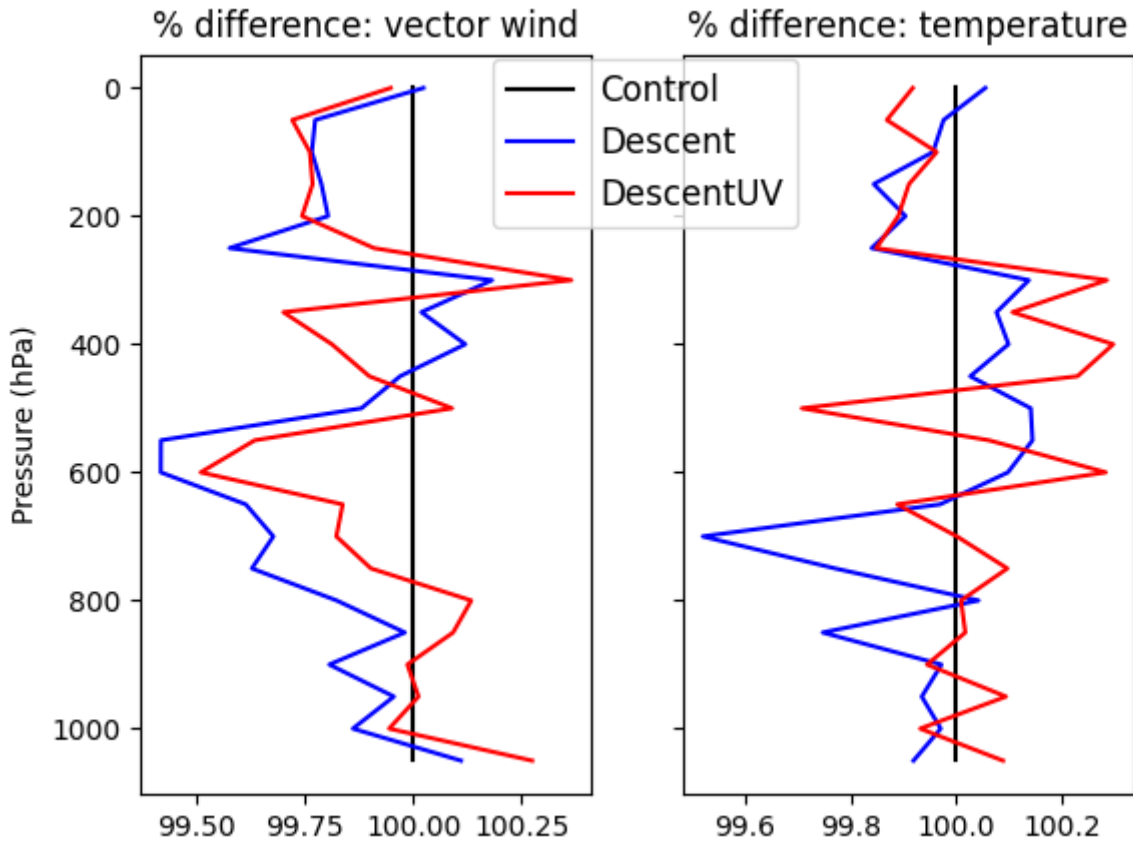
509

510   Figure 24. Effect of assimilation of all descent data (wind, temperature, humidity; blue line) or just descent winds (red line)

511   2020-01-20 to 2020-04-20. Results are shown for temperature and vector wind fit of 12 hour forecasts to European radiosonde

512   ascents, normalised by the fit of the control forecasts (so values less than 100% indicate improved forecasts).

513   **6 Discussion and conclusions**

514   The most obvious difference between ascent and descent data is that the descent temperatures are higher at upper levels. This

515   had been noted before for different radiosonde types, by Tiefenau and Gebbeken (1989) and Venkat Ratnam et al. (2014). Our

516   results suggest that the descent temperatures are too high and that this is closely linked to the descent rate (Figure 14). In Figure

517   17 the dependence on descent rate appears quadratic. Vaisala are working on updated processing to address the temperature

518   bias and other issues. There has been considerable discussion on the source of the ascent/descent temperature differences.

Whilst we cannot definitively explain the heating mechanism a plausible hypothesis is a conversion of kinetic energy via frictional heating. Clearly the falling radiosonde (plus balloon remains and parachute if fitted) are slowed by friction otherwise it would accelerate to much higher speeds during the descent. Future work might include testing radiosonde sensors in a wind tunnel with a flow of 20 m s^{-1} or more to see if the heating is replicated (care would be needed with the reference temperature). We have not been able to find such tests in the literature. There is a paper by de Podesta et al. (2018) about the effect of sensor diameter on temperature errors but they were looking at lower flow rates.

Another difference, that doesn't seem to have been reported before, is that on average the descent winds are smoother than the ascent winds. In part this is because ascents are generally more affected by pendulum motion, however inertial effects and the filtering applied to 'remove' pendulum motion also play a role. The smoother descent winds have a closer overall fit to the NWP winds, but we cannot currently say whether the ascent or descent winds are more accurate. Most studies of radiosondes concentrate on the temperatures and humidities and the winds are somewhat neglected; the use of long strings improves stratospheric temperatures at the expense of increasing the pendulum motions. For aircraft the winds have more than twice the impact of the temperatures on the quality of short-range forecasts (Ingleby et al, 2021) and forecast sensitivity diagnostics suggest that the same is true of radiosondes (Pauley and Ingleby, 2021), partly because satellite instruments primarily provide temperature and humidity data. Experience shows that GPS winds are generally good quality and biases do not seem to be a problem. GPS can provide high vertical resolution winds - but this makes pendulum motion more obvious and avoidance or removal of pendulum motion deserves more attention. One technique to obtain accurate wind profile data is the Jimsphere - a balloon with roughness elements used without a separate instrument package. Sako and Walterscheid (2016) discuss empirical filtering of wind profiles from radiosondes and Jimsphere balloons. Dropsonde wind profiles suffer much less from pendulum motion than radiosonde ascent winds (Wang et al, 2008) and probably less than radiosonde descent winds. The two balloon ascents of Kräuchi et al. (2016) largely eliminate pendulum motion but need more evaluation.

Some aspects of the descent data can be improved by estimating and removing heating effects due to high fall rates (on the temperature, and on the pressure for radiosondes without a pressure sensor). The descent characteristics are more variable than ascent rates in that for balloons with parachutes, how the parachute deploys can affect the amplitude of the pendulum motion and the descent speed. It is also likely that there can be improvements in the filtering of pendulum motion. Vaisala are working on these aspects but are not yet ready to give a timescale for changes. In principle users could apply bias corrections, but improving the winds is difficult if they have already been filtered. On the whole, it is simplest to stick to the current practice of manufacturers providing best estimate profiles, but more details of the processing would be welcome and this area should be kept under review. On a similar note there is a question of whether there should be a GRUAN descent product for the RS41 - more work on the uncertainties would be needed for this. There is the wider question of how much the lessons learnt from the RS41 descent are applicable to other radiosondes such as the Meteomodem M10. There is some evidence that pressure

552 sensor accuracy is worse whilst falling fast, but more work on this is needed. However the fall speed should have very little

553 effect on the accuracy of GPS derived positions, because the GPS satellites are moving much faster anyway.

554

555 There is evidence (Figure 13) that use of parachutes and/or pressure sensors gives some improvement to the descent data (the

556 benefits of parachutes or pressure sensors will reduce with improved processing/bias correction). There is also the possibility

557 of installing extra receivers to obtain more descent data from the lower troposphere (this has been demonstrated in Corsica,

558 Peyrat, pers. comm. 2020). Whether the extra costs are worthwhile would need to be assessed. We note that the impact of extra

559 radiosonde profiles over well-observed Europe will be less than the impact of extra profiles near remote islands or ships. In

560 May 2021 descent data was received from several European ships in the North Atlantic plus a station in Antarctica. ECMWF

561 and DWD have started operational assimilation of a subset of descent profiles - excluding the stratospheric segment with

562 higher average fall rates (it would be better to exclude data based on the actual descent rate, but this would require more work).

563 The US Navy global model is assimilating all available descent profiles (Pauley, pers. comm. 2021), we are not aware of other

564 NWP systems using them yet. NWP systems generally use pressure as the vertical coordinate for radiosonde data, arguably

565 there would be advantages in using height instead. There has been much more use of NWP model fields in this investigation

566 than is traditional for development/validation of in situ observations (but routine now for new satellites - Newman et al. 2020).

567 This means that a much larger sample can be examined. Note that traditional radiosonde intercomparisons (e.g., Nash et al,

568 2011) can't be used to assess descent data because the multi-radiosonde rig used has various implications for the descent

569 including possible entanglement. Descent data should be used with caution and sections with high descent rates particularly

570 so, however different users have different tolerances and we expect that improved processing will increase the proportion of

571 usable data.

7 Appendix: comparison with aircraft temperatures

573 For cruise level aircraft (typical speed is about 250 m s^{-1}) the measured temperature, known as total air temperature (TAT),

574 can be more than 20 K higher than the static air temperature (SAT). The link between TAT and SAT (Wendisch and Brenguier,

575 2013) can be expressed with equation:

576 $$SAT = \frac{TAT}{1+\frac{r(\gamma-1)}{2} \cdot M^2} \quad [A1],$$

577 where r is the recovery factor of the sensor, γ adiabatic index and M is Mach number.

578 From equation [A1] we can get the difference $TAT - SAT = SAT \cdot \frac{r(\gamma-1)}{2} \cdot M^2$

579 If we use the Mach number: $M = \frac{v}{a}$,

580 where v is the airspeed of the object (aircraft or radiosonde) and a the speed of sound, given by: $a = \sqrt{\gamma \cdot (C_p - C_v) \cdot SAT}$,

581   where C_p and C_v are heat capacity constants for constant pressure and volume respectively,

582   we can get: $TAT - SAT = \dfrac{r(\gamma-1)}{2} \cdot \dfrac{v^2}{\gamma \cdot (C_p - C_v)}$ [A2]

583   Applying $\gamma = \dfrac{C_p}{C_v}$ to equation [A2], the difference between measured and real temperature is:

584     $$TAT - SAT = \dfrac{v^2}{2C_p} r \qquad\qquad [A3],$$

585   According to the Wikipedia entry on Total air temperature, the typical recovery factor for platinum wire (which is used for

586   radiosondes) is 0.75 – 0.9. Even if we are not sure about the exact physical process of kinetic energy transfer to internal heat

587   in case of radiosondes, we might expect similar behavior (quadratic dependency on descent rate, but independent of height,

588   temperature and air density). When we apply the equation A3 to descending radiosondes, where v is the descent rate (DR) of

589   the radiosonde, with the range 0.75 - 0.9 for r we get:

590     $TAT - SAT = A \cdot 10^{-4} \cdot DR^2$ with A in the range 3.70 to 4.47.   [A4]

591   However, the similar coefficients for aircraft and descent radiosondes may come from different conversion mechanisms.

592

593   **Data availability statement**

594   The radiosonde descent data for September-November 2019 are available in BUFR format from

595   https://www.gruan.org/data/data-packages/dpkg-2021-2. Radiosonde ascent data in BUFR format are available from

596   https://www.ncei.noaa.gov/data/ecmwf-global-upper-air-bufr/ (see Geller et al, 2021, but note the change in URL). BUFR

597   decoding tools are available from ecCodes (with examples of radiosonde decoders at

598   https://confluence.ecmwf.int/display/ECC/bufr_read_tempf). Other decoders are also available, e.g.

599   https://github.com/NOAA-EMC/NCEPLIBS-bufr/tree/master .

600   **Author contributions**

601   BI with help from DE worked on paper conceptualization and on the methodology. BI, MM and GM performed the formal

602   analysis and visualisation. All the co-authors contributed to the writing of the paper, review and editing. Data curation was by

603   MS, BI and DE.

604   **Competing interests**

605   The authors declare that they have no conflict of interest.

606   **Acknowledgements**

607   The authors would like to thank the meteorological services that provided, and continue to provide, descent data. Michael de

608   Podesta (NPL) gave useful advice on the measurement of temperature by a moving sensor. Some early work on descent data

References

Bodeker, G. E., Bojinski, S., Cimini, D., Dirksen, R. J., Haeffelin, M., Hannigan, J. W., Hurst, D. F., Leblanc, T., Madonna, F., Maturilli, M., Mikalsen, A. C., Philipona, R., Reale, T., Seidel, D. J., Tan, D. G. H., Thorne, P. W., Vömel, H., and Wang, J.: Reference Upper-Air Observations for Climate: From Concept to Reality, B. Am. Meteorol. Soc. 97(1), 123-135. https://dx.doi.org/10.1175/BAMS-D-14-00072.1 2016.

de Podesta, M., Bell S., and Underwood R.: Air temperature sensors: dependence of radiative errors on sensor diameter in precision metrology and meteorology. Metrologia, 55, 229. 2018.

Dirksen, R. J., Sommer, M., Immler, F. J., Hurst D. F., Kivi R., and Vömel H.: Reference quality upper-air measurements: GRUAN data processing for the Vaisala RS92 radiosonde. Atmos. Meas. Tech., 7, 4463-4490, doi:10.5194/amt-7-4463-2014, 2014.

Geller, M. A., Love, P. T., Ingleby, B., and Yin, X.: New Availability of High Vertical-Resolution Radiosonde Data for Research New Availability of High Vertical-Resolution Radiosonde Data for Research. SPARC Newsletter, No 56, pp 14-15, https://www.sparc-climate.org/publications/newsletter/sparc-newsletter-no-56/, 2021.

Harrison, R.G. and Hogan, R.J.: In situ atmospheric turbulence measurement using the terrestrial magnetic field—a compass for a radiosonde. *J. Atmos. Ocean. Tech.*, *23*(3), pp.517-523. 2006.

Hock, T. F. and Franklin J. L.: The NCAR GPS Dropwindsonde. B. Am. Meteorol. Soc., 80, 407–420, https://doi.org/10.1175/1520-0477(1999)080<0407:TNGD>2.0.CO;2, 1999.

Hurst, D. H., Oltmans, S. J., Vömel, H., Rosenlof, K. H., Davis,S. M., Ray, E. A., Hall, E. G., and Jordan, A. F.: Stratospheric water vapor trends over Boulder, Colorado: Analysis of the 30 year Boulder record, J. Geophys. Res., 116, D02306,doi:10.1029/2010JD015065, 2011.

Ingleby, B.: An assessment of different radiosonde types 2015/2016. ECMWF Technical Memorandum 807. 2017.

Ingleby B., Isaksen, L., Kral, T., Haiden, T., and Dahoui, M.: Improved use of atmospheric *in situ* data. ECMWF Newsletter 155, pp 20-25 https://www.ecmwf.int/en/elibrary/18208-improved-use-atmospheric-situ-data 2018.

Ingleby, B., Candy, B., Eyre. J., Haiden, T., Hill, C., Isaksen, L., Kleist, D., Smith, F., Steinle, P., Taylor, S., Tennant, W., and Tingwell, C.: The impact of COVID-19 on weather forecasts: a balanced view. Geophys. Res. Lett. 2021.

Lomb, N.R. Least-squares frequency analysis of unequally spaced data. Astrophysics Space, 39(2):447–462, 1976.

Luers, J.K. and Eskridge, R.E. Use of radiosonde temperature data in climate studies. J. Climate, 11(5):1002–1019, 1998.

MacCready, P.B.: Comparison of Some Balloon Techniques. J. Appl. Meteorol., 4, 504-508, https://doi.org/10.1175/1520-0450(1965)004<0504:COSBT>2.0.CO;2, 1965.

Madonna, F., Kivi, R., Dupont, J.-C., Ingleby, B., Fujiwara, M., Romanens, G., Hernandez, M., Calbet, X., Rosoldi, M., Giunta, A., Karppinen, T., Iwabuchi, M., Hoshino, S., von Rohden, C., and Thorne, P. W.: Use of automatic radiosonde launchers to measure temperature and humidity profiles from the GRUAN perspective. Atmos. Meas. Tech., 13, 3621–3649, https://doi.org/10.5194/amt-13-3621-2020, 2020.

Marlton, G.J.. *On the development, characterisation and applications of a balloon-borne atmospheric turbulence sensor* (Doctoral dissertation, University of Reading). 2016.

Marlton, G.J., Giles Harrison, R., Nicoll, K.A. and Williams, P.D.: Note: A balloon-borne accelerometer technique for measuring atmospheric turbulence. *Rev. Sci. Instrum.*, *86*(1), p.016109. 2015.

Nash J., Oakley, T.,. Vömel, H., and Wei LI.: WMO Intercomparison of High Quality Radiosonde Systems Yangjiang, China, 12 July - 3 August 2010, WMO Instruments and Observing Methods Report No. 107. 2011.

Newman, S., Carminati, F., Lawrence, H., (...), Salonen, K., Bell, W.: Assessment of new satellite missions within the framework of numerical weather prediction. Remote Sensing 12(10), 1580, 2020.

Pauley P, and Ingleby B.: Assimilation of in-situ observations. In: Park SK, Xu L (eds) *Data Assimilation for Atmospheric, Oceanic and Hydrologic Applications (Vol. IV)*. Springer, in print. 2021.

Seidel DJ, Sun B, Pettey M, and Reale A.: Global radiosonde balloon drift statistics, J. Geophys. Res., 116 : D07102, doi:10.1029/2010JD014891. 2011.

Shepherd, T. G., Polichtchouk, I., Hogan R.J,.and Simmons A.J.: Report on Stratosphere Task Force. ECMWF Technical Memorandum 824. 2018.

Shimizu, K. and Hasebe, F.: Fast-response high-resolution temperature sonde aimed at contamination-free profile observations, Atmos. Meas. Tech., 3, 1673-1681, https://doi.org/10.5194/amt-3-1673-2010, 2010.

Söder, J., Gerding, M., Schneider, A., Dörnbrack, A., Wilms, H., Wagner, J., and Lübken, F.-J.: Evaluation of wake influence on high-resolution balloon-sonde measurements, Atmos. Meas. Tech., 12, 4191–4210, https://doi.org/10.5194/amt-12-4191-2019, 2019.

Tiefenau, H. K. E. and Gebbeken, A.: Influence of meteorological balloons on temperature measurements with radiosondes: night-time cooling and daytime heating. J. Atmos. Ocean. Tech., 6, 36-42, 1989.

Kräuchi A., Philipona, R., Romanens, G. Hurst, D.F., Hall, E.G.,and Jordan, A.F.: Controlled weather balloon ascents and descents for atmospheric research and climate monitoring. Atmos. Meas. Tech., 9, 929-938, doi:10.5194/amt-9-929-2016, 2016.

Vaisala: Vaisala RS41SG datasheet, *Vaisala* https://www.vaisala.com/sites/default/files/documents/WEA-MET-RS41-Datasheet-B211321EN.pdf 2017a.

Vaisala: Vaisala RS41 Radiosonde Measurement Performance white paper, https://www.vaisala.com/sites/default/files/documents/WEA-MET-RS41-Performance-White-paper-B211356EN-B-LOW-v3.pdf 2017b.

673 Venkat Ratnam, M., Pravallika, N., Ravindra Babu, S., Basha, G., Pramitha, M., and Krishna Murthy, B. V.: Assessment of
674 GPS radiosonde descent data, Atmos. Meas. Tech., 7, 1011-1025, 2014.

675 Wagner N.K.: Theoretical accuracy of a meteorological rocketsonde thermistor. J Appl. Meteorol, 3, 461-469, 1964.

676 Wang, J., Bian, J., Brown, W. O., Cole, H., Grubisic, V., and Young, K.: Vertical air motion from T-REX radiosonde and
677 dropsonde data, J. Atmos. Ocean. Tech., 26, 928-942, 2008.

678 Wendisch, M., and Brenguier, J.-L.: Airborne Measurements for Environmental Research: Methods and Instruments, Wiley,
679 641pp. 2013.

680 WMO: The difference in observed temperatures from radiosondes suspended 10 m and 40 m beneath a 1400 g balloon (J.B.
681 Elms, J. Nash and G. Williams). Papers Presented at the WMO Technical Conference on Instruments and Methods of
682 Observation (TECO-94), Instruments and Observing Methods Report No. 57,
683 WMO/TD-No. 588, Geneva, pp. 121-126. https://library.wmo.int/pmb_ged/wmo-td_588.pdf, 1994

684 WMO: Guide to Instruments and Methods of Observation, Vol I—Measurement of meteorological variables. WMO-No. 8,
685 548pp, https://library.wmo.int/doc_num.php?explnum_id=10179 2018a.

686 WMO: Guide to Instruments and Methods of Observation, Vol III—Observing Systems. WMO-No. 8, 426pp,
687 https://library.wmo.int/doc_num.php?explnum_id=9872 2018b.

688 WMO: Manual on Codes, Vol. I.2, Part B—Binary Codes and Part C—Common Features to Binary and Alphanumeric Codes.
689 WMO-No. 306, 1180 pp, https://library.wmo.int/doc_num.php?explnum_id=10310. 2019.

690 Zhang J, Chen H, Zhu Y, Shi H, Zheng Y, Xia X, Teng Y, Wang F, Han X, Li J, Xuan Y. A Novel Method for Estimating the
691 Vertical Velocity of Air with a Descending Radiosonde System. *Remote Sensing*. 11(13):1538.
692 https://doi.org/10.3390/rs11131538, 2019.

693